

An actin–myosin-II interaction is involved in maintaining the contractile ring in fission yeast

Masak Takaine<sup>§\*</sup>, Osamu Numata, Kentaro Nakano\*

Department of Biological Sciences, Graduate School of Life and Environmental Sciences,  
University of Tsukuba, 1-1-1 Tennohdai,  
Tsukuba, Ibaraki 305-8577, Japan.

§Present address: Gunma University Initiative for Advanced Research (GIAR), Gunma  
University, 3-39-15 Showa-machi, Maebashi, Gunma 371-8512, Japan.

\*To whom correspondence should be addressed: Masak Takaine (masaktakaine@gmail.com,  
Kentaro Nakano (knakano@biol.tsukuba.ac.jp, Phone/Fax: 81-029-853-6642)

Keywords: cytokinesis, contractile ring, fission yeast, myosin-II, actin cytoskeleton

## Abstract

The actomyosin-based contractile ring (CR), which assembles at the cell equator, maintains its circularity during cytokinesis in many eukaryotic cells, ensuring its efficient constriction. Although consistent maintenance of the ring is one of the mechanisms underpinning cytokinesis, it has not yet been fully addressed. We here investigated the roles of fission yeast myosin-II $s$  (Myo2 and Myp2/Myo3) in ring maintenance during cytokinesis, with a focus on Myo3. A site-directed mutational analysis showed that the motor properties of Myo3 were involved in its accumulation in the CR. Ring assembly was often deformable and not properly maintained under conditions in which the activities of myosin-II $s$  localizing to the CR were decreased, leading to inefficient cell division. Moreover, Myo3 appeared to form motile clusters on the ring. We proposed that large assemblies of myosin-II $s$  consolidated the CR by continuously binding to F-actin in the ring, thereby contributing to its maintenance.

## Introduction

After the completion of mitosis, one cell mechanically divides into two daughters, and this process is called cytokinesis. This coordinated cytofission ensures proper segregation of the genome and organelles, and its failure may induce changes in ploidy and oncogenesis or cell death (Ganem et al., 2007). Actin filaments (F-actin) and myosin-II both assemble into a circular structure along the cell equator, called the contractile ring (CR), during cytokinesis in many eukaryotic cells. In addition to large amounts of F-actin and myosin-II, the CR comprises various regulatory proteins such as actin-modulating proteins and signaling molecules, indicating the elaborate coordination of molecular systems (Eggert et al., 2006; Goyal et al., 2011). Similar to the contraction of muscle sarcomeres, bipolar myosin-II filaments are considered to slide F-actin in opposite orientations closer together in order to drive shrinkage of the CR, which, in turn, generates the inward force required for cortical ingression during cytokinesis (Wang, 2005; Pollard, 2010). This is called the purse-string model and is consistent with previous findings showing that CR F-actin had mixed polarities (Sanger and Sanger, 1980; Maupin and Pollard, 1986; Kamasaki et al., 2007). The number of sarcomere-like contractile units in the unconstricted CR of *Caenorhabditis elegans* embryos has been suggested to reflect the scalability of the ring constriction rate: larger rings constrict faster than smaller ones (Carvalho et al., 2009).

Although a previous study suggested the involvement of the motor activity of myosin-II in the constriction of the CR or cytokinesis (Straight et al., 2003), the precise configuration of actin and myosin-II in the ring and the mechanism by which the local actin-myosin interaction is harnessed for global shrinkage have yet to be elucidated. The motor activity of myosin-II has also been shown to promote the turnover of cortical actin during cytokinesis (Guha et al., 2005; Murthy and Wadsworth, 2005), which is suggestive of its function in actin disassembly. Myosin-II was previously shown to induce the disintegration of F-actin bundles

*in vitro* and has been implicated in cellular actin network disassembly (Haviv et al., 2008; Wilson et al., 2010). Moreover, motor-impaired mutant myosin-IIIs have been shown to effectively support cytokinesis (Reichl et al., 2008; Ma et al., 2012), suggesting that myosin-II modulates cortical tension by crosslinking F-actin rather than sliding F-actin in the CR during cytokinesis.

Two myosin-II isoforms in *Schizosaccharomyces pombe*, Myo2 and Myo3 (also called Myp2), both localize to the CR and have been implicated in cytokinesis. Myo2 is essential for cell proliferation, whereas the function of Myo3 is vital for growth under certain conditions. During metaphase, the anillin-related protein Mid1 recruits Myo2 to the medial cortex as a broad band of nodes in an F-actin-independent manner, possibly via an interaction with the C-terminal tail moiety of Myo2 (Motegi et al., 2004). The motor activity of Myo2 has been suggested to drive the capture and pulling of F-actin elongated from the nodes, leading to the coalescence of these nodes and F-actin into a ring (Vavylonis et al., 2008), which indicates the primary role of Myo2 in ring assembly. Myo3 is a single-headed myosin-II with a large gap in the coiled-coil region (Fig. 1A) and localizes to the ring following the completion of its assembly depending on F-actin (Wu et al., 2003). A double mutation of *myo3* $\Delta$  (a null mutation in *myo3*) and the *myo2-EI* (a temperature-sensitive allele of *myo2* (Balasubramanian et al., 1998)) were previously shown to cause more severe defects in cytokinesis (Motegi et al., 2000). The motor heads of Myo2 and Myo3 are assumed to have similar properties because they were found to be functionally exchangeable (Bezanilla and Pollard, 2000). Thus, although the two myosin-IIIs have been suggested to play an overlapping role, possibly via their head moieties, the underlying mechanism currently remains unclear. As Myo3 is single-headed, it is currently unclear whether and how it may be involved in CR constriction, whereas Myo2 may assemble into bipolar filaments and contribute to ring constriction through the purse-string mechanism. Additionally, previous

studies have indicated the role of Myo3 in cell division under high-chloride ion environments. The molecular bases of the chloride tolerance of Myo3 and its relationship to the shared function with Myo2 also have not yet been elucidated.

In the present study, we focused on Myo3 in order to examine the role of myosin-II following CR assembly. Myo3 localized to the CR following the assembly of the actin ring, depending solely on F-actin. A site-directed mutational analysis revealed that the motor properties of Myo3 were implicated in its localization to the medial region. Under conditions in which the local accumulation of Myo3 and motor activity of Myo2 were both reduced, the CR that assembled was not maintained properly in some fractions of cells, resulting in inefficient septation, which suggested the collaborative role of the myosin-IIs in maintaining the ring. Moreover, Myo3 appeared to form motile clusters on the ring. We proposed that large assemblies, bipolar filaments, or clusters of myosin-IIs consolidated the CR by continuously binding to F-actin in the ring, thereby cooperatively contributing to its maintenance during cytokinesis.

## Results

### Myo3 localized to the CR by solely depending on actin filaments

We recently reported that the CR of the fission yeast *S. pombe* consisted of the F-actin-dependent and -independent fractions of several ring components, even after the completion of ring assembly (Takaine et al., 2014a). mYFP-Myo2 colocalized with F-actin in the medial region as a node structure at early anaphase and as a ring at late anaphase (Fig. 1B). The localization of Lifeact was homogenous in cells treated with Latrunculin-A (Lat-A), indicating the disassembly of cellular F-actin structures into undetectable actin subunits. Myo2 localized as medial cortical dots distinguished from precursor nodes in the absence of F-actin (Fig. 1B, arrowheads), which was consistent with our previous findings. We then

attempted to determine whether another myosin-II, Myo3, in the CR was also composed of the F-actin-dependent and -independent fractions. The Lat-A-induced disappearance of F-actin and localization of Myo3 were examined by time-lapse imaging. Myo3 and actin colocalized in the CR at late anaphase. The exposure of cells to a low concentration of DMSO did not affect maintenance or constriction of the ring (Fig. 1C and Movie 1). The addition of Lat-A disintegrated the actin-Myo3 ring and other F-actin structures within several minutes, suggesting that an F-actin-independent fraction was not present in the Myo3 ring (Fig. 1D and Movie 2). The decrease in fluorescence intensity in these rings was favorably fit by a single exponential function. The half-decline time of Myo3 was slightly smaller than that of actin (1.6 vs. 3.5 min;  $p = 0.001$ ). The disassembly of F-actin in the constricting ring similarly caused dispersion of the Myo3 signal (Fig. 1E). These results suggested that CR F-actin was the primary and essential scaffold for Myo3 through cytokinesis.

### **Myo3 gradually accumulated on F-actin in the CR**

We simultaneously examined the accumulation kinetics of Myo3 and actin to the equatorial ring. In early anaphase, actin gradually accumulated at the cell middle, forming a thin ring (Fig. 2A and Movie 3). As the actin ring thickened at late anaphase, the Myo3 signal began to increase in the medial region (Fig. 2B-C). The actin and Myo3 rings held together in place for several minutes (dwell time of the ring), and then constricted in a synchronized manner. Myo3 localized only very slightly to the F-actin net as the precursor of the actin ring (Fig. 2D). Deconvolution microscopy revealed that the actin rings were almost continuous, suggesting that the concentration of actin in the CR was constant, whereas Myo3 rings were more inhomogeneous and discontinuous (Fig. 2E). Myo3 may preferentially localize to a limited number of sites on the actin ring. We further examined the formation of Myo3 and

actin rings in *mid1* $\Delta$  cells, in which the CR is assembled from strands, not from medial nodes (Saha and Pollard, 2012). In these cells, actin appeared as strands and assembled into a ring, and Myo3 formed a ring after the actin ring assembled (Fig. 2F-G). Thus, Myo3 may specifically interact with F-actin, which is almost assembled into a ring independently of Mid1.

### **Mutations in the motor moiety altered the local concentration of Myo3**

The F-actin-dependent localization of Myo3 to the CR implied that Myo3 interacted with F-actin in the ring via its motor domain. In order to investigate the relationship between the motor properties of Myo3 and its localization, we introduced several well-characterized point mutations into the highly conserved regions in the head moiety (Figs. 3A-B and S1), which took advantage of *myo3* not being required for viability in contrast to *myo2*. An immunoblot analysis demonstrated that these mutants were produced at the same level as wt (Fig. 3C). The E480K mutant corresponded to one of the mutant myosins that showed no detectable ATPase activity and actin filament sliding (Ruppel and Spudich, 1996). Myo3-E480K-3mYFP, which was expected to have no ATPase activity, showed no ring localization at anaphase (Fig. 3D). The R240A mutant Myo3 was predicted to have low actin-activated ATPase activity and not drive F-actin sliding since the original mutant myosin-II had a  $V_{\max}$  value one-fifth that of wt, a  $K_m$  value 2.5-fold higher than that of wt, and also showed no motility (Shimada et al., 1997). Although Myo3-R240A localized to the CR, its local concentration decreased to 15% that of wt (Fig. 3D-E). The S469V mutant presumably corresponded to a mutant myosin that retained high actin-activated ATPase activity, but translocated F-actin at only one-tenth the speed of wt (indicating the uncoupling of ATPase activity and motility) (Ruppel and Spudich, 1996; Endow, 2000). The local concentration of Myo3-S469V in the CR was approximately half that of wt (Fig. 3 D-E). The R702C/R709C

mutants of human non-muscle myosin IIA/B showed approximately 20% of the maximum actin-activated ATPase activity of wt and had a higher affinity for actin in the presence of ATP (its  $K_m$  value was less than one-third that of wt) due to the very slow release of ADP (Kim et al., 2005). Moreover, the motilities of the mutant myosins were severely impaired (Hu et al., 2002; Kim et al., 2005). The local concentration of the corresponding Myo3-R694C mutant in the ring was 1.8-fold higher than that of wt (Fig. 3 D-E). The G680V mutant myosin-II of *Dictyostelium discoideum* strongly bound to actin even in the presence of ATP by possibly forming a stable actin–myosin-II complex carrying ADP and phosphate (Uyeda et al., 2002). The bulk of the corresponding Myo3-G688V mutant formed an aggregate in the medial region, while the rest localized faintly to the CR (Fig. 3D). The aggregates were distinct from SPBs and often persisted during interphase (Fig. 3F). These results suggested that (1) an undisturbed ATP hydrolysis cycle was required for the proper distribution of Myo3 over the ring and that (2) the affinity for F-actin in the presence of ATP was relevant for its local concentration. The motility of Myo3 itself did not appear to be essential for its localization.

We also examined the localization of the C-terminal tail (aa 827–2104) of Myo3. Myo3tail-3mYFP expressed under the control of the *nmt41* promoter diffused over the cytoplasm, whereas full-length Myo3 expressed under the same promoter localized to the CR (Fig. 3G). This result again suggested that Myo3 localized to the cytokinetic actin ring in a manner that depended on its head moiety.

Myo3-null cells showed a morphological phenotype in the presence of high concentrations of the chloride ion, possibly because of the failure of cytokinesis (Bezanilla et al., 1997; Motegi et al., 1997). Therefore, we investigated the chloride ion sensitivity of mutant myo3 strains. Cells from E480K, R240A, G688V, and myo3tail mutants were often multi-septated and swollen in 1 M KCl, similar to *myo3Δ* cells, while cells from *myo3*<sup>+</sup>,

S469V, and R694C strains showed no morphological defects (Fig. 3H). Therefore, the function of *myo3*<sup>+</sup> to maintain cell morphology under high chloride ion conditions may require its local concentrations at the CR to be higher than the minimum level, and did not appear to correlate with its motor activity.

### **Accumulation kinetics of mutant Myo3s during cytokinesis**

We hereafter examined the S469V and R694C mutants because they did not exhibit the KCl phenotype, but had a lower or higher local concentration, respectively, than wt. We observed the accumulation of wt or mutant Myo3 together with Rlc1, a light chain of myosin-II, during cytokinesis. Rlc1 labeled Myo2 and Myo3, and visualized the course of CR assembly from a band of cortical nodes in the medial region. The wt Myo3 formed a medial ring approximately 15 min after the Rlc1 ring had assembled (Fig. 4A, D and Movie 4). Myo3-R694C accumulated on the CR earlier than wt and decelerated constriction of the ring (Fig. 4B, D, E and Movie 4). Myo3-S469V accumulated on the ring with kinetics similar to those of wt; however, its local amount was markedly lower, and did not interfere with ring constriction (Fig. 4C-E). Neither of the mutant Myo3s retarded the cell growth (Fig. 4F) or assembly of the CR, as monitored by Rlc1 localization (Fig. 4D) in *myo2*<sup>+</sup> strains. These results suggested that binding sites for Myo3 on the ring were available after the completed assembly of the ring, and diffused Myo3 molecules directly bound to the sites rather than migrating toward the ring via ring-associated actin tracks (Arai and Mabuchi, 2002; Huang et al., 2012).

### **Myo3 was involved in the constriction rate of the CR and septation efficiency**

The deceleration of ring constriction by the Myo3-R694C mutant implied the involvement of Myo3 in ring constriction during cytokinesis under normal conditions, as reported recently

(Arasada and Pollard, 2014), not only under severe conditions (Bezanilla et al., 1997; Motegi et al., 1997). Therefore, we re-examined the phenotypes of *myo3Δ* under normal growth conditions. The percentage of singly septated cells was significantly higher in an asynchronous culture of *myo3Δ* than in wt, suggesting prolonged cell division (Fig. S2A-B). We also observed that the rate of constriction of the CR in *myo3Δ* cells was significantly lower (80%) than that in wt cells, whereas the time required for ring assembly and the dwell time of the CR were similar in both strains (Fig. S2C-E). These results implicated Myo3 in the constriction of the CR and, hence, showed that it was required for efficient septation under normal conditions.

### **Stable localization of Myo3 to the CR was required for its maintenance in the *myo2-E1* background**

In order to understand the function of Myo3 in cytokinesis in more detail, we examined motor-impaired *myo3* mutants in the *myo2-E1* background, a temperature-sensitive mutant strain of *myo2* that showed severe defects in CR assembly at a restrictive temperature (Balasubramanian et al., 1998) and slower assembly and constriction of the ring at a permissive temperature (Stark et al., 2010). Biochemically, the mutant Myo2 had significantly diminished ATPase activities and was unable to drive the gliding of F-actin, but bound to filaments under restricted diffusion conditions (Stark et al., 2013). We generated *myo2/myo3* double mutants and observed CR assembly at 25°C. In *myo2-E1 myo3<sup>+</sup>* cells, the assembly and constriction of the CR were both slower than those in *myo2<sup>+</sup>* cells (compare Figs. 4A, D-E and 5A, E-F). Prolonged ring assembly also delayed the localization of Myo3 to the CR. In *myo2-E1 myo3-R694C* cells, constriction of the CR was retarded more than that in *myo2-E1* cells, indicating that Myo2-E1 and Myo3-R694C additively affected ring constriction (Fig. 5B, E-F). Myo3-R694C localized to the CR earlier than Myo3, as observed

in *myo2*<sup>+</sup> cells. Although Myo3-S469V-3mYFP localized to the CR in the *myo2-E1* background, its signal was very susceptible to photobleaching (Fig. S3A), and, thus, we were unable to precisely determine when the Myo3-S469V ring was formed. The CR constricted slower in 44% of *myo2-E1 myo3-S469V* cells than in *myo2-E1* cells (Fig. 5C-F and Movie 5). In half of the cells, the signal of the Rlc1 ring gradually degraded after late anaphase, and septation was retarded (Fig. 5C-D, G and Movie 6). This was unusual because more than 95% of cells in the *myo2-E1* and *myo2-E1 myo3-R694C* strains showed constriction of the ring, and no ring degradation was observed. Furthermore, the rings that assembled were deformed in 45% of *myo3-S469V* cells (arrowheads in Fig. 5C, H-I). Correspondingly, the growth of *myo2-E1 myo3-S469V* cells was slightly slower (Fig. 4F). The CR assembled with similar kinetics among these three strains. These results suggested that the motor activities of Myo2 and Myo3 were jointly involved in maintaining the CR after anaphase.

We also examined the behavior of the actin ring in *myo2-E1 myo3-S469V* cells (Fig. S3). Most *myo2-E1* cells septated after the medial actin ring constricted. The actin ring constricted more slowly in 50% of *myo2-E1 myo3-S469V* cells than in *myo2-E1* cells, and delayed septation occurred. In the remaining cells, the actin ring assembled, but then decondensed into fragments, and septation was also retarded. Collectively, we concluded that actin and myosin-II structures in the CR may both be decomposed in half of the *myo2-E1 myo3-S469V* cells. Taken together, these results suggested that catalytically active myosin-II motors contributed the maintenance of actin and myosin structures in the CR.

### ***cdc8* genetically interacted with *myo3***

Cdc8 is the single tropomyosin of fission yeast and essential for cytokinesis and organization of the actin cytoskeleton (Balasubramanian et al., 1992; Chang et al., 1996), and has been shown to localize to F-actin cables and the CR (Arai et al., 1998). Biochemically,

Cdc8 stabilizes F-actin, enhances the association between Myo2 and F-actin, and promotes the actin-activated ATPase activities of Myo2 (Stark et al., 2010). Therefore, we generated and examined a double mutant bearing both *myo3* $\Delta$  and *cdc8-110*, a temperature-sensitive mutant of *cdc8* (Nurse et al., 1976). Under all permissive temperatures tested, *myo3* $\Delta$  *cdc8-110* cells grew more slowly than wt and single mutants (Fig. S4A). Moreover, the number of multinucleated cells was significantly higher in the double mutant than in the others (Fig. S4B). These results indicated that *myo3* and *cdc8* were synergistically involved in cytokinesis and cell growth and were consistent with previous findings (Motegi et al., 1997). We also examined the assembly and constriction of the CR in the double mutant under permissive conditions. The time required for assembly of the CR was longer in *cdc8-110* and *myo3* $\Delta$  *cdc8-110* cells, by approximately 7 min, than in wt or *myo3* $\Delta$  cells (Fig. 6A-B, D), suggesting no cooperativity between *myo3* and *cdc8* for ring assembly. However, there appeared to be significant cooperativity for ring constriction and ring maintenance. The ring constricted very slowly in 32% of the double mutant cells, whereas in most of the wt, *myo3* $\Delta$ , and *cdc8-110* cells the ring constricted much faster (Fig. 6C, E-F). In 44% of *myo3* $\Delta$  *cdc8-110* cells, the ring persisted for an abnormally long time (at least 70 min, the maximum lifetime of the CR in wt) without constriction (Fig. 6C, E-F). This long-lasting ring was also observed in 4% of *cdc8-110* cells. The ring disappeared after an unusually prolonged duration without constriction in 20% of the double mutant cells (Fig. 6E-F and Movie 7). In addition, 35% of *myo3* $\Delta$  *cdc8-110* cells displayed a deformed CR after its assembly (Fig. 6G-H), which was not observed in other strains or resembled *myo2-E1 myo3-S469V* cells. These results suggested that *myo3* cooperated with *cdc8* to properly maintain the CR after late anaphase, and were partially supportive of the aforementioned hypothesis that myosin motors contributed to maintaining the CR.

### Myo3 formed motile clusters on the ring

We attempted to elucidate the mechanism responsible for maintaining the CR by Myo3. Fluorescence recovery after the photobleaching (FRAP) analysis revealed that Myo3 at the CR was largely immobile and turned over relatively slowly (Fig. 7A-B), which indicated the stable localization of Myo3 and was consistent with its function as a ring stabilizer. Myo3-R694C had a smaller mobile fraction and turned over more slowly than wt, again suggesting that ATP hydrolysis correlated with the dissociation of Myo3 from the ring.

In order to gain further insights into the behavior of Myo3, we investigated the discontinuous signals of Myo3-3mYFP at the CR (as already described in Fig. 2) using time-lapse imaging. The signals of Myo3-3mYFP gradually accumulated as dozens of fine dots along the actin ring and formed a discontinuous ring (Fig. 7C). Hereafter, we referred to these dots as Myo3 clusters. These clusters were constantly motile and their fluorescence intensities varied (Fig. 7D and Movie 8). A kymographic analysis revealed that Myo3 clusters continually emerged and disappeared with an average lifetime of 29 s and were capable of moving in both directions (Fig. 7F). Myo3-R694C-3mYFP formed slightly more clusters than wt, and they had significantly longer lifetimes (Fig. 7E-F; see also Movie 8), which was consistent with their higher local concentrations and low mobility.

We constructed several deletion forms of Myo3-3mYFP (Fig. 7G) in order to identify the regions involved in the clustering or localization of Myo3. The C-terminal coiled-coil region spanning 500 aa was dispensable for localization to the CR and cluster formation (Fig. 7H). Deletions including the central region of the tail moiety (corresponding to 1248–1615 aa) significantly decreased the medial accumulation of Myo3: Myo3-1048 localized as dim puncta along the equator, and Myo3-1247 and Myo3-827 sometimes accumulated as several dots in the medial region. We also found that the moderate expression of Myo3-1248-1615-3mYFP did not localize to the CR (Fig. 7I). When overexpressed, Myo3-1248-1615 localized

weakly to the equator in late anaphase cells. Most of the deletion forms of Myo3-3mYFP localized similarly in *myo2-E1* strains (Fig. S4D), which may minimize the possibility of their recruitment through interactions with Myo2. Taken together, these results suggested that Myo3 molecules formed multimeric complexes on the CR and the medial localization of Myo3 depended on the motor domain and central region of the tail.

We then investigated the biochemical properties of Myo3-1248-1615 using a sedimentation assay. GST-Myo3-1248-1615 alone partially sedimented, whereas GST did not (Fig. 8A). F-actin significantly increased the amount of sedimentable GST-Myo3-1248-1615 (Fig. 8B). These results indicated that Myo3-1248-1615 was more likely to form large aggregates or interacted with F-actin weakly with an apparent  $K_d$  of  $7 \pm 2 \mu\text{M}$ .

## Discussion

### **Motor properties of Myo3 were relevant to its distribution over the ring and local concentration**

The contribution of the motor domain of myosin-II to its localization to the cleavage furrow (CF) or the CR had previously been unclear because the accumulation of myosin-II to the CF or CR was typically concurrent with its filamentogenesis and depended heavily on the tail moiety, but not on the motor domain (Dean et al., 2005). Some scaffold proteins may tether the rod of myosin-II filaments to the equatorial cortex in these cells. In the present study, we showed that Myo3 localized to the CR by solely depending on F-actin through cytokinesis and its motor properties were relevant to its accumulation. The local concentrations of mutant Myo3s (R240A, -E480K, and -R694C) correlated with the affinity of the head for F-actin in the presence of ATP, as represented by the  $K_m$  value. The reduced local concentration of Myo3-S469V may also have been due to its lower affinity for F-actin because a similar

uncoupling mutant S456L appeared to have a higher  $K_m$  value for actin than that of wt (Murphy et al., 2001). In addition, the clumping of Myo3-G688V suggested that an uninterrupted ATP hydrolysis cycle was required for uniform distribution along the ring. In contrast, the motility of the mutant Myo3 did not appear to directly correlate with its localization. A cycle of ATP hydrolysis by myosin-II is coupled to a cycle of attachment to and detachment from F-actin. Thus, disassociation by ATP hydrolysis from F-actin rather than motility may be essential for spreading Myo3 over the CR. All the point-mutations introduced into Myo3 were located outside the actin-binding face of the motor domain and, hence, were less likely to directly alter its affinity for F-actin.

The motor domain of Myo2 solely localized to the CR (Lord et al., 2005), and Myo3-1048 also accumulated along the ring, suggesting the specific association of myosin-II motor domains with CR F-actin. One possible mechanism for this is the preferential binding of myosin-II motor domains to mechanically stretched F-actin (Uyeda et al., 2011). Myo3 was hardly detectable on precursor medial reticular F-actin, whereas it accumulated along the sharp actin ring, which implied that the configuration or tension of the equatorial F-actin affected its affinity for Myo3. The inefficient equatorial accumulation of Myo3-827 in the *myo2-E1* strain (in which tension could be weakened) may also support this idea.

Alternatively, actin-binding proteins associating with CR F-actin may increase the affinity of myosin-II for actin, as previously reported for Cdc8 (Stark et al., 2010).

### **Myo3 cooperated with Myo2 and Cdc8 to maintain the actin ring after late anaphase**

The motor activity of myosin-II may drive the shrinkage of interdigitated F-actin in the CR (the purse-string model). Our results suggested that myosin-II motor activity was also vital for maintaining the CR, providing a new perspective regarding the functions of myosin-II in cytokinesis (Fig. 8C). Maintenance of the CR evidently underpins its constriction because

destabilization, or even disassembly, of the ring either before or during constriction is unfavorable. After being joined to the ring at late anaphase, Myo3 may collaborate with Myo2 in its maintenance and constriction. Based on the functional equivalency of the motor heads between Myo3 and Myo2 (Bezanilla and Pollard, 2000), the two myosin-IIs may work in parallel using a similar mechanism. Since half of the *myo2-E1 myo3-S469V* cells displayed constriction of the CR, while the other half did not, a minimum requirement (watershed) appears to exist for ring-localized myosin-II motor activity that is proportional to their local concentrations and specific ATPase activities for maintenance of the ring. The amount of myosin-II activity may be very close to the minimum in these cells. Since *myo3-S469V* cells did not exhibit a morphological phenotype in 1 M KCl, similar to *myo3Δ* cells, maintenance of the CR may be the primary role of Myo3, which may be separate from its tolerance to high concentrations of the chloride ion. By assuming that some signaling cascade is activated under high-chloride ion conditions, Myo3 may provide a scaffold for signal transduction in which signaling molecules interact, as already speculated (Bezanilla and Pollard, 2000).

We also found that maintenance of the CR was compromised in *cdc8-110 myo3Δ* cells, in which the activity of myosin-IIs was presumably reduced. Cdc8 may indirectly enhance the actin–myosin interaction and ATPase activity of Myo2 (and possibly Myo3) in order to properly maintain the CR after late anaphase. Double mutant cells also displayed unusual persistence of the CR. The small fraction of *cdc8-110* cells with a long-lasting ring indicated that the initiation of ring constriction was mechanically unfavorable, which may be exaggerated in combination with *myo3Δ*. We speculated that Cdc8 also stabilized the actin ring via direct binding in order to maintain the ring to some extent and promote transition from the dwell phase to constriction.

### Possible mechanisms responsible for maintaining the actin ring by Myo3

A previous study demonstrated that the recombinant Myo3 tail was monomeric because it formed an intramolecular coiled-coil and, hence, Myo3 was a single-headed myosin-II (Bezanilla and Pollard, 2000). Meanwhile, CR-localized Myo3 may be in large assemblies because most of the Myo3 signal appeared as dozens of motile puncta. We also found that the motor domain of Myo3 and central region of its tail were both weakly localized to the medial cortex at late anaphase, and both were required for sufficient accumulation. Myo3 appeared to interact superficially with the actin ring rather than being integrated into the ring considering its concentration behind the actin ring. These results prompted us to speculate that Myo3 molecules on the actin ring formed clusters with their tails, which associated with a kernel (Fig. 8D). As the local amount of Myo3 was estimated to be 2,000 molecules (Wu and Pollard, 2005), each cluster may comprise several tens of Myo3 molecules. The Myo3 cluster may be able to sustain continuous attachment to the CR F-actin and crosslink them, circumferentially or transversely, as it has multiple motor domains. The multivalent attachment of Myo3 clusters may contribute to consolidation of the actin ring. A FRAP analysis revealed the slow turnover rate and low mobility of ring-localized Myo3, which may be explained by its preferential incorporation into the clusters. Meanwhile, single-headed Myo3 was not expected to interact with F-actin as persistently because it was presumed to have a very low duty ratio. Thus, clustered Myo3 may be suitable machinery permitting single-headed myosin-II to maintain the CR by associating stably with the actin ring.

The molecular entity of cluster kernels remains unknown. The transmembrane protein Chs2 localized to the medial region during septation and co-immunoprecipitated with Myo3 (Martín-García and Valdivieso, 2006). However, since Myo3 localized to the CR in *chs2Δ* cells, Chs2 may not provide a strong anchor for Myo3. Myo3-1248-1615 may be directly involved in clustering on the actin ring because this moiety was liable to form aggregates,

and F-actin may facilitate aggregation. Since these properties and cellular localization appear to differ from those of the entire tail ((Bezanilla and Pollard, 2000); Fig. 3G), this region may be structurally masked by other regions. Posttranslational modifications (*e.g.*, phosphorylation) may relieve this masking.

Myo3-R694C maintained the CR as effectively as Myo3 in the *myo2-E1* background, suggesting that the association between myosin-II and F-actin may be more important for maintenance of the ring than their ATPase activity or motility. This is reminiscent of the situation in COS-7 cells (Ma et al., 2012) in which the mutant non-muscle myosin-II, NMHC IIB-R709C (equivalent to the R694C alternation), was able to support cytokinesis; however, it had significantly reduced ATPase activity and was unable to translocate F-actin. The proposal that bipolar myosin-II filaments are required not for its motor activity to glide F-actin, but as an active actin crosslinker to generate cortical tension, which drives cytokinesis, appeared to be consistent with our results. Moreover, our results were compatible with studies using *Dictyostelium* or protoplasts of fission yeast showing that the CR maintained local cortical tension, but did not limit the speed of constriction (Reichl et al., 2008; Stachowiak et al., 2014). The greater importance of the local concentration of Myo3 over its motor activity for ring maintenance also supports this idea. One of the common roles of myosin-II in eukaryotic cell cytokinesis may be in the relocatable crosslinking of F-actin, which enables tension to be exerted on cortical F-actin, including the CR, to maintain the ring.

On the other hand, Myo3-R694C dominantly reduced the rate of CR constriction, suggesting that Myo3 itself is involved in ring constriction. Excessive consolidation of the ring via Myo3 clusters and Myo2 filaments may decelerate ring constriction. Conversely, the knockdown of alpha-actinin, a longer actin crosslinker that localized to the CF, accelerated cytokinesis in NRK cells (Mukhina et al., 2007). Therefore, local concentrations of different types of actin crosslinkers may coordinately determine the optimal constriction rate of the CR.

## Materials and Methods

### Yeast strains and genetic manipulations

The fission yeast strains used in this study are listed in Table S1. These strains were constructed by a PCR-based-gene-targeting method, PCR sewing technique (Bähler et al., 1998; Matsuyama et al., 2000), and genetic crosses. The plasmids used in this study are listed in Tables S2. Cells were grown in complete yeast extract medium YES or in minimal medium EMM with auxotrophic supplements. Cells were grown to mid-log at 25°C before imaging unless otherwise noted.

In order to precisely determine the localization of Myo3, we integrated three tandem copies of the monomeric yellow fluorescent protein (mYFP, a monomeric variant of YFP with an A206K mutation) at the C-terminus of the *myo3* chromosomal locus. A *3mYFP-hphMX6* module flanked by homologous sequences (400–500 bp) was amplified using MTP19 (Takaine et al., 2014a) as a template for this purpose. The DNA fragment was transformed into the wt strain MTY10, and transformants were selected for hygromycin resistance. Myo3-3mYFP fusion was fully functional. In order to generate tail-truncated mutant strains of *myo3*, MTY1001, 1002, 1003, 1008, and 1004, *3mYFP-hphMX6* modules were amplified using appropriate primers, as described above, and inserted after amino acids 1990, 1615, 1247, 1048, and 827 of endogenous *myo3*, respectively.

Point mutations were created by oligonucleotide-directed mutagenesis using a TAKARA mutagenesis kit (TaKaRa) and appropriate primers on a plasmid carrying the *myo3*<sup>+</sup> gene, MTP467 (Motegi et al., 1997), to generate mutant *myo3-3mYFP* strains. All plasmids were sequenced to confirm PCR fidelity. In a *myo3-3mYFP* strain (MTY465), a region of the *myo3* gene (corresponding to 400–2400 bp) was replaced with a *ura4*<sup>+</sup> module, yielding strain MTY672. A *myo3* fragment, corresponding to 0–4000 bp, carrying a point mutation was linearized by a *PstI/ScaI* cut of the mutagenized plasmid (MTP461, 465, 466,

486, or 487) and subjected to the transformation of MTY672. Colonies were selected for uracil auxotrophy on a plate containing 5-fluoroorotic acid. Correct integrations were confirmed by diagnostic PCR and sequencing.

## Microscopy

Single time-point and epifluorescence microscopy was performed using an inverted fluorescence microscope (BX51; Olympus) equipped with a Plan-Apo 100×/1.40 NA objective lens (Olympus) using U-MNIBA3 and U-MWIG3 filters (Olympus) and a cooled charge-coupled device (CCD) camera (ORCAII-ER-1394; Hamamatsu Photonics) using SimplePCI software (Compix, Inc.) at room temperature. Time-lapse imaging was performed under a confocal microscope (LSM 700; Carl Zeiss, Inc.) equipped with an alpha Plan-Apochromat 100×/1.46 NA objective lens (Carl Zeiss, Inc.) or using an inverted fluorescence microscope (BX71; Olympus) equipped with a UPlanSApo 100×/1.40 NA objective lens (Olympus), spinning-disk confocal scanner (CSU22; Yokogawa), piezo objective positioner (E-665; Physik Instrumente), and electron multiplying CCD camera (iXon 3 885; Andor) with excitation by 488-nm and 568-nm lasers using GFP and mCherry filters and MetaMorph software (version 7.7.5.0; Molecular Devices) at 25°C. In the latter system, simultaneous two-color imaging was performed using an emission beam splitter (Dual View; Roper Scientific). Cells for time-lapse imaging were typically immobilized on pads made from 20% gelatin and 5% low-melting agarose in media, or directly mounted on a slide for single time point observations. Stacks of 12–17 confocal  $z$ -sections spaced by 0.3–0.5  $\mu\text{m}$  were typically collected. Confocal  $z$ -sections were sometimes deconvolved using Huygens Essential software (version 4.5; Scientific Volume Imaging) based on the classic maximum likelihood estimation method. In order to distinguish ring signal degradation in *myo2-E1 myo3-S469V* cells from global fluorescence decay due to photobleaching during imaging, we only scored

the cells that showed the signal disappearance of the Rlc1-3mCherry ring before the mean fluorescence intensity at each frame of the time-lapse image was significantly decreased due to photobleaching. Through this study, mitotic progression was monitored by the separation of spindle pole bodies (SPBs) labeled by Sid4-3mYFP, indicating elongation of the spindle. The images shown are maximum projections to an  $xy$  image of  $z$ -stacks unless otherwise noted.

In time-lapse imaging of motile Myo3 clusters on the CR, the signals of myo3-3mYFP were imaged by collecting nine confocal  $z$ -sections spaced by 0.31  $\mu\text{m}$  through only the lower half of the cell with a 15-s interval using the inverted fluorescence microscope equipped with the CSU22 spinning-disk confocal scanner (see above). Each  $z$ -section was an average of two images. The images were deconvolved to explicitly visualize each cluster. In order to compare the mean number of clusters on the ring in *myo3-3mYFP* and *myo3-R694C-3mYFP* cells, we semi-automatically detected clusters using the find maxima function of ImageJ. The number of clusters detected in each frame was averaged across all (29–36) frames.

We manually selected tracks in kymographs to measure the lifetimes of clusters and only further analyzed clusters that met the following criteria: (1) brighter than the background signals; (2) discriminative from neighboring signals; (3) almost spherical; (4) having an almost constant signal intensity through its duration.

### **FRAP measurements**

Fluorescence recovery after the photobleaching (FRAP) analysis was performed using LSM 700 at 25°C. Stacks of 13  $z$ -sections spaced by 0.5  $\mu\text{m}$  were collected with a 20-s interval. Each  $z$ -section was an average of two images scanned using 0.5% laser power at 488 nm. Photobleaching was performed at 80% laser power by 20 iterative scanning in a circular

region (20 pixels diameter) of the ring. Each  $z$ -stack was projected to an  $xy$  image using Image J and the sum intensity projection procedure. The mean fluorescence intensity of the ring region was measured, subtracted by the background value (an average of two cytoplasmic regions), and normalized to the prebleach fluorescence intensity (an average of two time points before photobleaching). Data were further corrected for acquisition bleaching using the function,  $I_t = I_\infty + (I_0 - I_\infty) \times \exp(-k_{\text{decay}} \times t)$ , where  $t$  is time,  $I_t$  is the normalized intensity at time point  $t$ ,  $I_\infty$  is the normalized intensity at an infinite time point, and  $k_{\text{decay}}$  indicates a decay constant. The decay function was calculated by fitting the data from the unbleached ring regions using Kaleidagraph software (Synergy Software). The resultant recovery curve was fit with a single exponential function,  $I_t = I_\infty + (I_0 - I_\infty) \times \exp(-k \times t)$ , where  $I_0$  is the normalized intensity just after bleaching, and  $k$  is the recovery rate constant closely related to the dissociation rate constant. The mobile fraction and half time for recovery were calculated according to the equations  $MF = (I_\infty - I_0) / (I_\infty - I_0)$  and  $\tau_{1/2} = \ln 2 / k$ , respectively.

### Quantitative fluorescence microscopy

Myo3-3mYFP ring intensities were quantified as previously described (Takaine et al., 2014a). In brief, we imaged *myo3-3mYFP sid4-3mYFP* cells in 13  $z$ -sections at 0.38- $\mu\text{m}$  intervals using the spinning disk confocal microscope averaging two images. The stack of  $z$ -sections was projected to an  $xy$  image using the sum intensity projection method of ImageJ. We then measured the mean fluorescence intensities of two SPBs and the medial rings in late anaphase cells. Regions of interests were a circle of 0.64  $\mu\text{m}$  (8 pixels) in diameter for one SPB and a rectangle of 0.5–1  $\mu\text{m}$  (6–12 pixels)  $\times$  2.4–4.0  $\mu\text{m}$  (30–50 pixels) for the ring, respectively. After background subtraction, the total ring intensity was normalized to the average intensity of Sid4-3mYFP at SPBs in the cell.

### **Actin depolymerization assay using Latrunculin-A**

Cells for time lapse imaging were adsorbed onto the surface of a 35-mm glass-bottom dish coated with lectin (L-2320, Sigma) for 10 min. The immobilized cells were imaged by collecting stacks of 12 *z*-sections spaced by 0.42  $\mu\text{m}$  at 0.5- or 1-min intervals. During the interval after the second stack was acquired, the culture was supplemented with 0.36% DMSO alone or 0.36% DMSO and 5  $\mu\text{M}$  Lat-A by the manual addition of an equal volume (approximately 50  $\mu\text{l}$ ) of the 2 $\times$  concentrated solution. These cells were subsequently imaged until the signal of F-actin disappeared. The mean fluorescence intensity of the medial region was measured, subtracted by the background value, and normalized to the pretreatment fluorescence intensity. Using Kaleidagraph software, the normalized decline curve was fit with a single exponential function.

### **Immunoblotting**

Total cell lysates were prepared from mid-log cells as described previously (Takaine et al., 2014b). Proteins were resolved by SDS-5–20% PAGE on a precast gel (C520L, ATTO) and transferred to a polyvinylidene difluoride membrane (Immobilon-P; Millipore). YFP and  $\alpha$ -tubulin were probed using an anti-GFP antibody (Roche) and the anti-tubulin antibody TAT-1 (Woods et al., 1989), respectively.

### **Actin sedimentation assay**

Monomeric rabbit skeletal muscle actin, bacterially expressed recombinant GST, and GST-Myo3-1248-1615 were prepared as described previously (Takaine et al., 2009) and clarified by centrifugation at 200,000  $\times g$  for 20 min. Samples containing 4  $\mu\text{M}$  actin and 0–6.3  $\mu\text{M}$  GST-Myo3-1248-1615 in KMEI (0.1 M KCl, 2 mM MgCl<sub>2</sub>, 0.5 mM EGTA, 0.5 mM DTT, 0.2 mM ATP, and 10 mM imidazole-HCl, pH 7.5) were incubated for 30 min at 25°C,

centrifuged at  $200,000 \times g$  for 15 min, and the supernatants and pellets obtained were then subjected for SDS-PAGE. The gels were stained with Coomassie blue, and bands were quantified by densitometry using Image J software.

### **Statistical analysis**

Means, SDs, and  $p$ -values were calculated using Excel software (Microsoft). Error bars denote SD unless otherwise noted. Significance between two sets of data was tested using an unpaired one-tailed Welch's  $t$ -test. These  $p$ -values were in bold type if the value was less than 0.05. Significance was also indicated by an asterisk. Box plots show the 75th and 25th percentiles of the data (interquartile range) as the upper and lower edges of the box, the median as the medial line in the box, the  $1.5 \times$  interquartile range as whiskers, and outliers as circles.

### **Supplementary material**

Supplementary material is available online at xxxxx

### **Acknowledgments**

We are grateful to the Yeast Genetic Resource Center (Osaka City University) for providing yeast strains.

### **Author contributions**

M. T. and K. N. designed the research with contributions from O. N. M. T. conducted the experiments. M. T. wrote the manuscript with contributions from all other authors.

## Funding

This work was supported by JSPS KAKENHI Grant Numbers 24770177 to M. T., 24570207 to K. N, 24657128 to O. N.

## References

- Arai, R. and Mabuchi, I.** (2002). F-actin ring formation and the role of F-actin cables in the fission yeast *Schizosaccharomyces pombe*. *J Cell Sci* **115**, 887-898.
- Arai, R., Nakano, K. and Mabuchi, I.** (1998). Subcellular localization and possible function of actin, tropomyosin and actin-related protein 3 (Arp3) in the fission yeast *Schizosaccharomyces pombe*. *Eur J Cell Biol* **76**, 288-295.
- Arasada, R. and Pollard, T. D.** (2014). Contractile ring stability in *S. pombe* depends on F-BAR protein Cdc15p and Bgs1p transport from the Golgi complex. *Cell Rep* **8**, 1533-1544.
- Bähler, J., Wu, J. Q., Longtine, M. S., Shah, N. G., McKenzie III, A., Steever, A. B., Wach, A., Philippsen, P. and Pringle, J. R.** (1998). Heterologous modules for efficient and versatile PCR-based gene targeting in *Schizosaccharomyces pombe*. *Yeast* **14**, 943-951.
- Balasubramanian, M. K., Helfman, D. M. and Hemmingsen, S. M.** (1992). A new tropomyosin essential for cytokinesis in the fission yeast *S. pombe*. *Nature* **360**, 84-87.
- Balasubramanian, M. K., McCollum, D., Chang, L., Wong, K. C., Naqvi, N. I., He, X., Sazer, S. and Gould, K. L.** (1998). Isolation and characterization of new fission yeast cytokinesis mutants. *Genetics* **149**, 1265-1275.
- Bezanilla, M. and Pollard, T. D.** (2000). Myosin-II tails confer unique functions in *Schizosaccharomyces pombe*: characterization of a novel myosin-II tail. *Mol Biol Cell* **11**, 79-91.
- Bezanilla, M., Forsburg, S. L. and Pollard, T. D.** (1997). Identification of a second myosin-II in *Schizosaccharomyces pombe*: Myp2p is conditionally required for cytokinesis. *Mol Biol Cell* **8**, 2693-2705.
- Carvalho, A., Desai, A. and Oegema, K.** (2009). Structural memory in the contractile ring makes the duration of cytokinesis independent of cell size. *Cell* **137**, 926-937.
- Chang, F., Woollard, A. and Nurse, P.** (1996). Isolation and characterization of fission yeast mutants defective in the assembly and placement of the contractile actin ring. *J Cell Sci* **109** ( Pt 1), 131-142.
- Dean, S. O., Rogers, S. L., Stuurman, N., Vale, R. D. and Spudich, J. A.** (2005). Distinct pathways control recruitment and maintenance of myosin II at the cleavage furrow during cytokinesis. *Proc Natl Acad Sci U S A* **102**, 13473-13478.
- Eggert, U. S., Mitchison, T. J. and Field, C. M.** (2006). ANIMAL CYTOKINESIS: From Parts List to Mechanisms. *Annu Rev Biochem* **75**, 543-566.
- Endow, S. A.** (2000). Molecular motors--a paradigm for mutant analysis. *J Cell Sci* **113** ( Pt 8), 1311-1318.
- Ganem, N. J., Storchova, Z. and Pellman, D.** (2007). Tetraploidy, aneuploidy and cancer. *Curr Opin Genet Dev* **17**, 157-162.
- Goyal, A., Takaine, M., Simanis, V. and Nakano, K.** (2011). Dividing the spoils of growth and the cell cycle: The fission yeast as a model for the study of cytokinesis. *Cytoskeleton (Hoboken)* **68**, 69-88.

- Guha, M., Zhou, M. and Wang, Y. L.** (2005). Cortical actin turnover during cytokinesis requires myosin II. *Curr Biol* **15**, 732-736.
- Haviv, L., Gillo, D., Backouche, F. and Bernheim-Groswasser, A.** (2008). A cytoskeletal demolition worker: myosin II acts as an actin depolymerization agent. *J Mol Biol* **375**, 325-330.
- Hu, A., Wang, F. and Sellers, J. R.** (2002). Mutations in human nonmuscle myosin IIA found in patients with May-Hegglin anomaly and Fechtner syndrome result in impaired enzymatic function. *J Biol Chem* **277**, 46512-46517.
- Huang, J., Huang, Y., Yu, H., Subramanian, D., Padmanabhan, A., Thadani, R., Tao, Y., Tang, X., Wedlich-Soldner, R. and Balasubramanian, M. K.** (2012). Nonmedially assembled F-actin cables incorporate into the actomyosin ring in fission yeast. *J Cell Biol* **199**, 831-847.
- Kamasaki, T., Osumi, M. and Mabuchi, I.** (2007). Three-dimensional arrangement of F-actin in the contractile ring of fission yeast. *J Cell Biol* **178**, 765-771.
- Kim, K. Y., Kovács, M., Kawamoto, S., Sellers, J. R. and Adelstein, R. S.** (2005). Disease-associated mutations and alternative splicing alter the enzymatic and motile activity of nonmuscle myosins II-B and II-C. *J Biol Chem* **280**, 22769-22775.
- Lord, M., Laves, E. and Pollard, T. D.** (2005). Cytokinesis depends on the motor domains of myosin-II in fission yeast but not in budding yeast. *Mol Biol Cell* **16**, 5346-5355.
- Ma, X., Kovács, M., Conti, M. A., Wang, A., Zhang, Y., Sellers, J. R. and Adelstein, R. S.** (2012). Nonmuscle myosin II exerts tension but does not translocate actin in vertebrate cytokinesis. *Proc Natl Acad Sci U S A* **109**, 4509-4514.
- Martín-García, R. and Valdivieso, M. H.** (2006). The fission yeast Chs2 protein interacts with the type-II myosin Myo3p and is required for the integrity of the actomyosin ring. *J Cell Sci* **119**, 2768-2779.
- Matsuyama, A., Yabana, N., Watanabe, Y. and Yamamoto, M.** (2000). *Schizosaccharomyces pombe* Ste7p is required for both promotion and withholding of the entry to meiosis. *Genetics* **155**, 539-549.
- Maupin, P. and Pollard, T. D.** (1986). Arrangement of actin filaments and myosin-like filaments in the contractile ring and of actin-like filaments in the mitotic spindle of dividing HeLa cells. *J Ultrastruct Mol Struct Res* **94**, 92-103.
- Motegi, F., Nakano, K. and Mabuchi, I.** (2000). Molecular mechanism of myosin-II assembly at the division site in *Schizosaccharomyces pombe*. *J Cell Sci* **113** ( Pt 10), 1813-1825.
- Motegi, F., Mishra, M., Balasubramanian, M. K. and Mabuchi, I.** (2004). Myosin-II reorganization during mitosis is controlled temporally by its dephosphorylation and spatially by Mid1 in fission yeast. *J Cell Biol* **165**, 685-695.
- Motegi, F., Nakano, K., Kitayama, C., Yamamoto, M. and Mabuchi, I.** (1997). Identification of Myo3, a second type-II myosin heavy chain in the fission yeast *Schizosaccharomyces pombe*. *FEBS Lett* **420**, 161-166.
- Mukhina, S., Wang, Y. L. and Murata-Hori, M.** (2007). alpha-Actinin Is Required for Tightly Regulated Remodeling of the Actin Cortical Network during Cytokinesis. *Dev Cell* **13**, 554-565.
- Murphy, C. T., Rock, R. S. and Spudich, J. A.** (2001). A myosin II mutation uncouples ATPase activity from motility and shortens step size. *Nat Cell Biol* **3**, 311-315.
- Murthy, K. and Wadsworth, P.** (2005). Myosin-II-dependent localization and dynamics of F-actin during cytokinesis. *Curr Biol* **15**, 724-731.
- Nurse, P., Thuriaux, P. and Nasmyth, K.** (1976). Genetic control of the cell division cycle in the fission yeast *Schizosaccharomyces pombe*. *Mol Gen Genet* **146**, 167-178.

- Patterson, B., Ruppel, K. M., Wu, Y. and Spudich, J. A.** (1997). Cold-sensitive mutants G680V and G691C of Dictyostelium myosin II confer dramatically different biochemical defects. *J Biol Chem* **272**, 27612-27617.
- Pollard, T. D.** (2010). Mechanics of cytokinesis in eukaryotes. *Curr Opin Cell Biol* **22**, 50-56.
- Reichl, E. M., Ren, Y., Morphew, M. K., Delannoy, M., Effler, J. C., Girard, K. D., Divi, S., Iglesias, P. A., Kuo, S. C. and Robinson, D. N.** (2008). Interactions between myosin and actin crosslinkers control cytokinesis contractility dynamics and mechanics. *Curr Biol* **18**, 471-480.
- Ruppel, K. M. and Spudich, J. A.** (1996). Structure-function studies of the myosin motor domain: importance of the 50-kDa cleft. *Mol Biol Cell* **7**, 1123-1136.
- Saha, S. and Pollard, T. D.** (2012). Anillin-related protein Mid1p coordinates the assembly of the cytokinetic contractile ring in fission yeast. *Mol Biol Cell* **23**, 3982-3992.
- Sanger, J. M. and Sanger, J. W.** (1980). Banding and polarity of actin filaments in interphase and cleaving cells. *J Cell Biol* **86**, 568-575.
- Shimada, T., Sasaki, N., Ohkura, R. and Sutoh, K.** (1997). Alanine scanning mutagenesis of the switch I region in the ATPase site of Dictyostelium discoideum myosin II. *Biochemistry* **36**, 14037-14043.
- Stachowiak, M. R., Laplante, C., Chin, H. F., Guirao, B., Karatekin, E., Pollard, T. D. and O'Shaughnessy, B.** (2014). Mechanism of cytokinetic contractile ring constriction in fission yeast. *Dev Cell* **29**, 547-561.
- Stark, B. C., Sladewski, T. E., Pollard, L. W. and Lord, M.** (2010). Tropomyosin and myosin-II cellular levels promote actomyosin ring assembly in fission yeast. *Mol Biol Cell* **21**, 989-1000.
- Stark, B. C., James, M. L., Pollard, L. W., Sirotkin, V. and Lord, M.** (2013). UCS protein Rng3p is essential for myosin-II motor activity during cytokinesis in fission yeast. *PLoS One* **8**, e79593.
- Straight, A. F., Cheung, A., Limouze, J., Chen, I., Westwood, N. J., Sellers, J. R. and Mitchison, T. J.** (2003). Dissecting temporal and spatial control of cytokinesis with a myosin II Inhibitor. *Science* **299**, 1743-1747.
- Takaine, M., Numata, O. and Nakano, K.** (2009). Fission yeast IQGAP arranges actin filaments into the cytokinetic contractile ring. *EMBO J* **28**, 3117-3131.
- Takaine, M., Numata, O. and Nakano, K.** (2014a). Fission yeast IQGAP maintains F-actin-independent localization of myosin-II in the contractile ring. *Genes Cells* **19**, 161-176.
- Takaine, M., Imada, K., Numata, O., Nakamura, T. and Nakano, K.** (2014b). The meiosis-specific nuclear passenger protein is required for proper assembly of forespore membrane in fission yeast. *J Cell Sci* **127**, 4429-4442.
- Uyeda, T. Q., Tokuraku, K., Kaseda, K., Webb, M. R. and Patterson, B.** (2002). Evidence for a novel, strongly bound acto-S1 complex carrying ADP and phosphate stabilized in the G680V mutant of Dictyostelium myosin II. *Biochemistry* **41**, 9525-9534.
- Uyeda, T. Q., Iwadate, Y., Umeki, N., Nagasaki, A. and Yumura, S.** (2011). Stretching actin filaments within cells enhances their affinity for the myosin II motor domain. *PLoS One* **6**, e26200.
- Vavylonis, D., Wu, J. Q., Hao, S., O'Shaughnessy, B. and Pollard, T. D.** (2008). Assembly mechanism of the contractile ring for cytokinesis by fission yeast. *Science* **319**, 97-100.
- Wang, Y. L.** (2005). The mechanism of cortical ingression during early cytokinesis: thinking beyond the contractile ring hypothesis. *Trends Cell Biol* **15**, 581-588.

- Wilson, C. A., Tsuchida, M. A., Allen, G. M., Barnhart, E. L., Applegate, K. T., Yam, P. T., Ji, L., Keren, K., Danuser, G. and Theriot, J. A.** (2010). Myosin II contributes to cell-scale actin network treadmilling through network disassembly. *Nature* **465**, 373-377.
- Woods, A., Sherwin, T., Sasse, R., MacRae, T. H., Baines, A. J. and Gull, K.** (1989). Definition of individual components within the cytoskeleton of *Trypanosoma brucei* by a library of monoclonal antibodies. *J Cell Sci* **93** ( Pt 3), 491-500.
- Wu, J. Q. and Pollard, T. D.** (2005). Counting cytokinesis proteins globally and locally in fission yeast. *Science* **310**, 310-314.
- Wu, J. Q., Kuhn, J. R., Kovar, D. R. and Pollard, T. D.** (2003). Spatial and temporal pathway for assembly and constriction of the contractile ring in fission yeast cytokinesis. *Dev Cell* **5**, 723-734.

## Figures

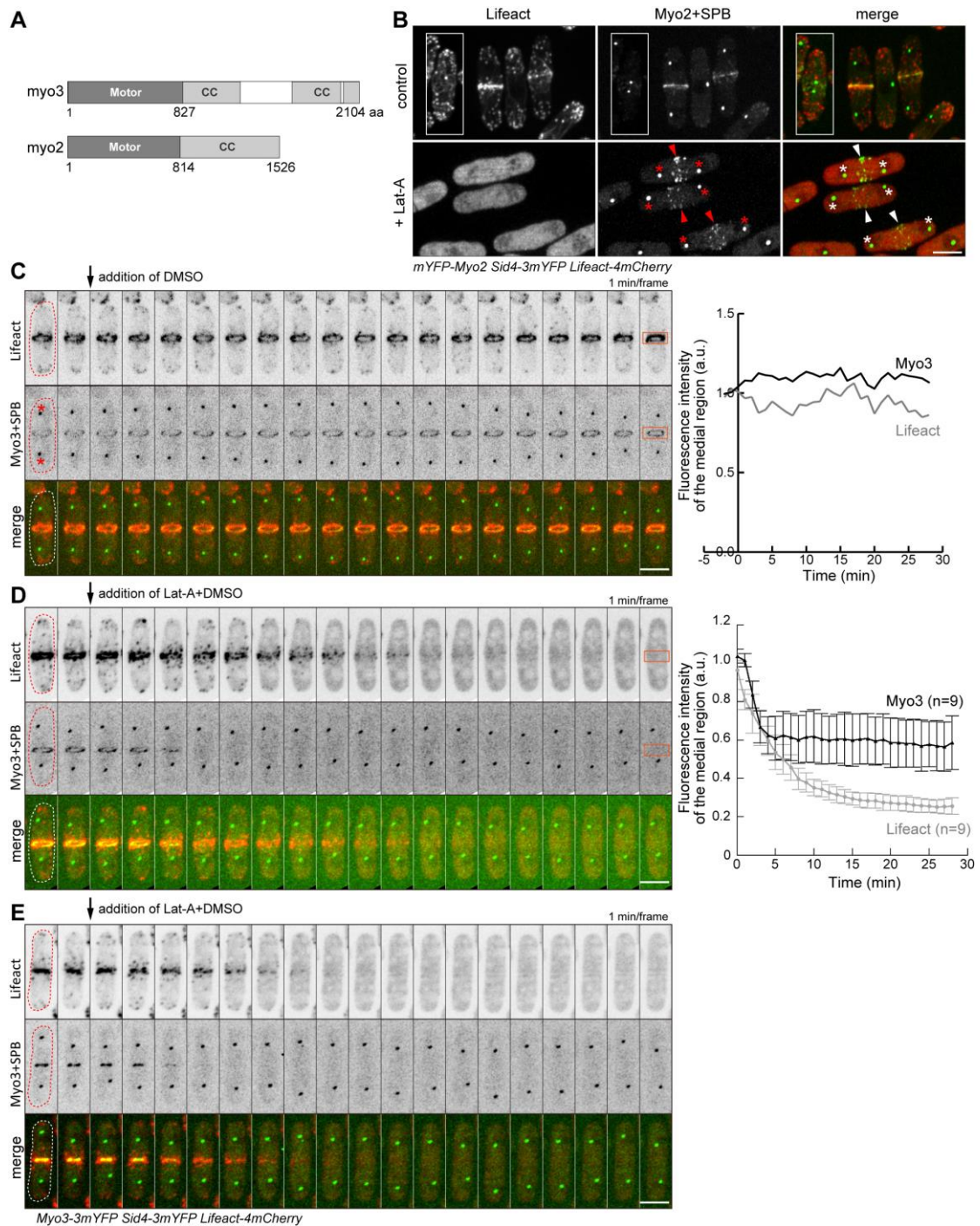


**Fig. 1. Localization of Myo3 to the CR depended on F-actin through cytokinesis**

(A) Structures of Myo3 and Myo2. CC, coiled-coil region. (B) Cells treated with 0.25% DMSO plus 0 or 8  $\mu$ M Lat-A for 20 min. Arrowheads indicate some of the F-actin-independent cortical dots of mYFP-Myo2. Insets show a cell bearing the medial node

structures of mYFP-Myo2. (C-E) Time-lapse imaging of Myo3-3mYFP rings. Myo3, Lifeact and SPBs in late anaphase cells were simultaneously imaged at 1-min intervals. DMSO (0.36%) alone (C) or DMSO plus 7  $\mu$ M Lat-A (D) was supplemented at the indicated time-points. *Right*, Mean fluorescence intensities of boxed regions plotted over time. Data in (D) are the mean  $\pm$  SD (error bars), and pooled from two independent experiments. (E) Cells having constricting rings were similarly treated with Lat-A. Asterisks indicate some SPBs for clarity. Bars, 5  $\mu$ m.

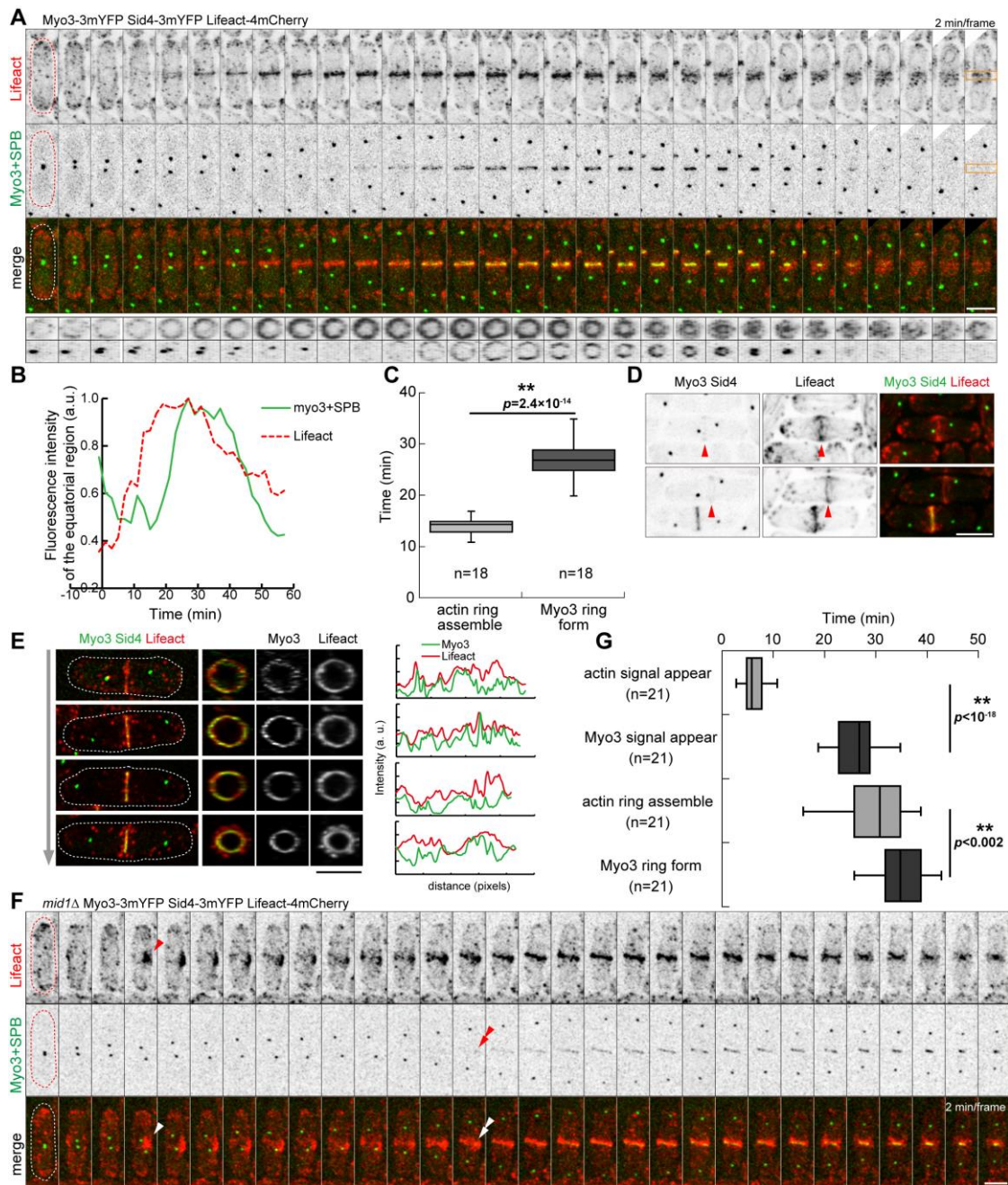


**Fig. 2. Myo3 gradually localized to the CR during actin ring assembly**

(A) Simultaneous observation of Myo3 and actin during assembly and constriction of the CR.

*Bottom*, images obtained from 90° rotation of the medial region. (B) Mean fluorescence intensities of a boxed region in (A) were plotted over time. SPB separation was set as  $t = 0$ .

(C) Box plot of times required for the assembly of actin and Myo3 rings from SPB separation.

Data were pooled from two independent preparations. (D) Myo3 scarcely localized to the

actin ring under construction. The precursor fine F-actin was visualized by higher speed image acquisition. Arrowheads indicate unassembled actin rings. Note that a very weak signal of Myo3-3mYFP in unassembled actin rings may not have been detected in (A) due to the higher detection limit of the system used. (E) An orthogonal view of Myo3 and actin rings. Cells at progressive stages of Myo3 accumulation were imaged with higher spatial resolution. *Right*, line profiles of actin and Myo3 fluorescence intensities along the circumference. (F) Simultaneous observation of Myo3 and actin during cytokinesis in *mid1* $\Delta$  cells. An arrowhead indicates the appearance of a clump of actin strands. A double arrowhead indicates appearance of the Myo3 signal. (G) Box plot of times required for the assembly of actin and Myo3 rings in *mid1* $\Delta$  cells. Data were pooled from three independent preparations. A double asterisk indicate a significant difference ( $p < 0.01$ ). Bars, 5  $\mu$ m.

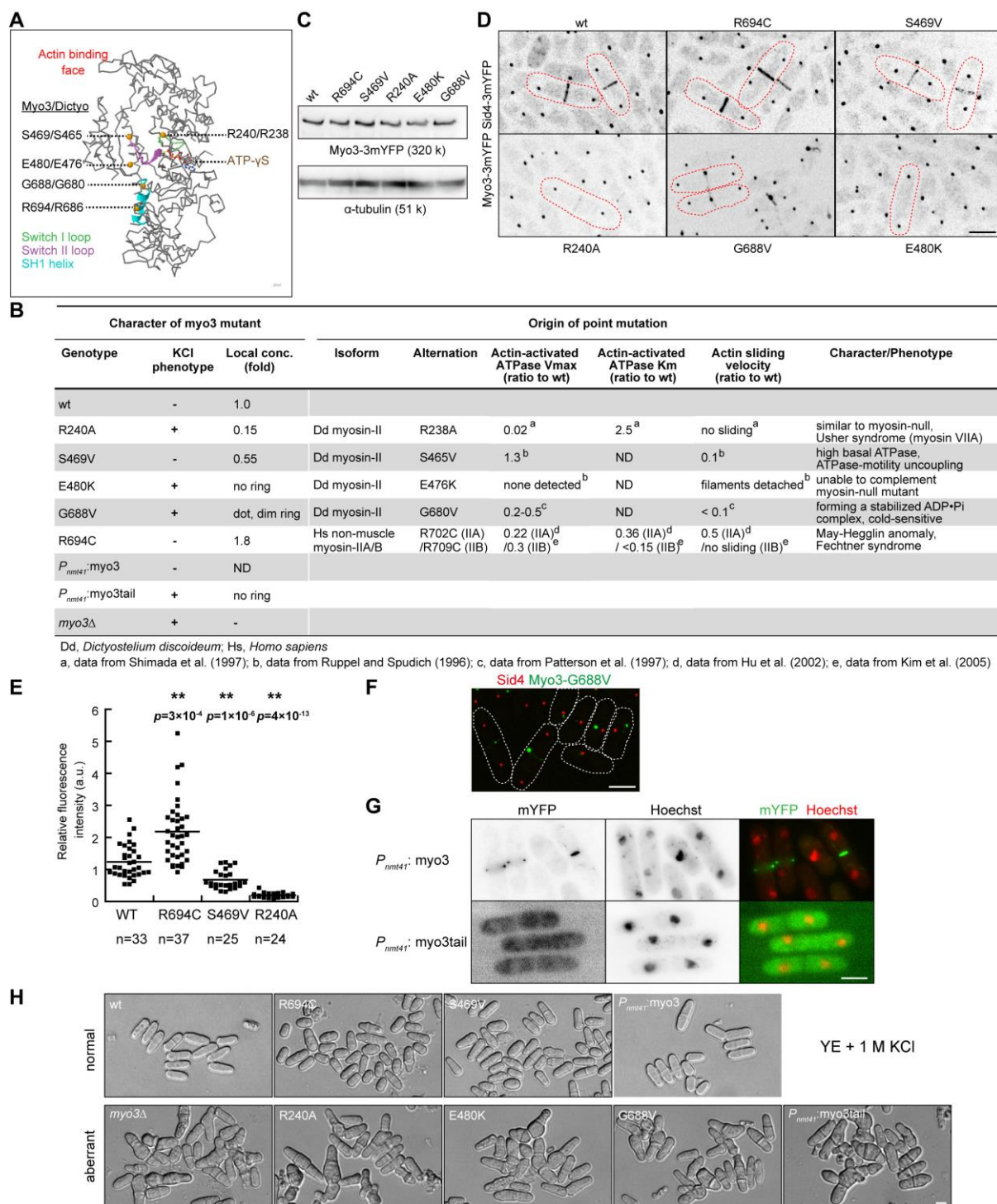
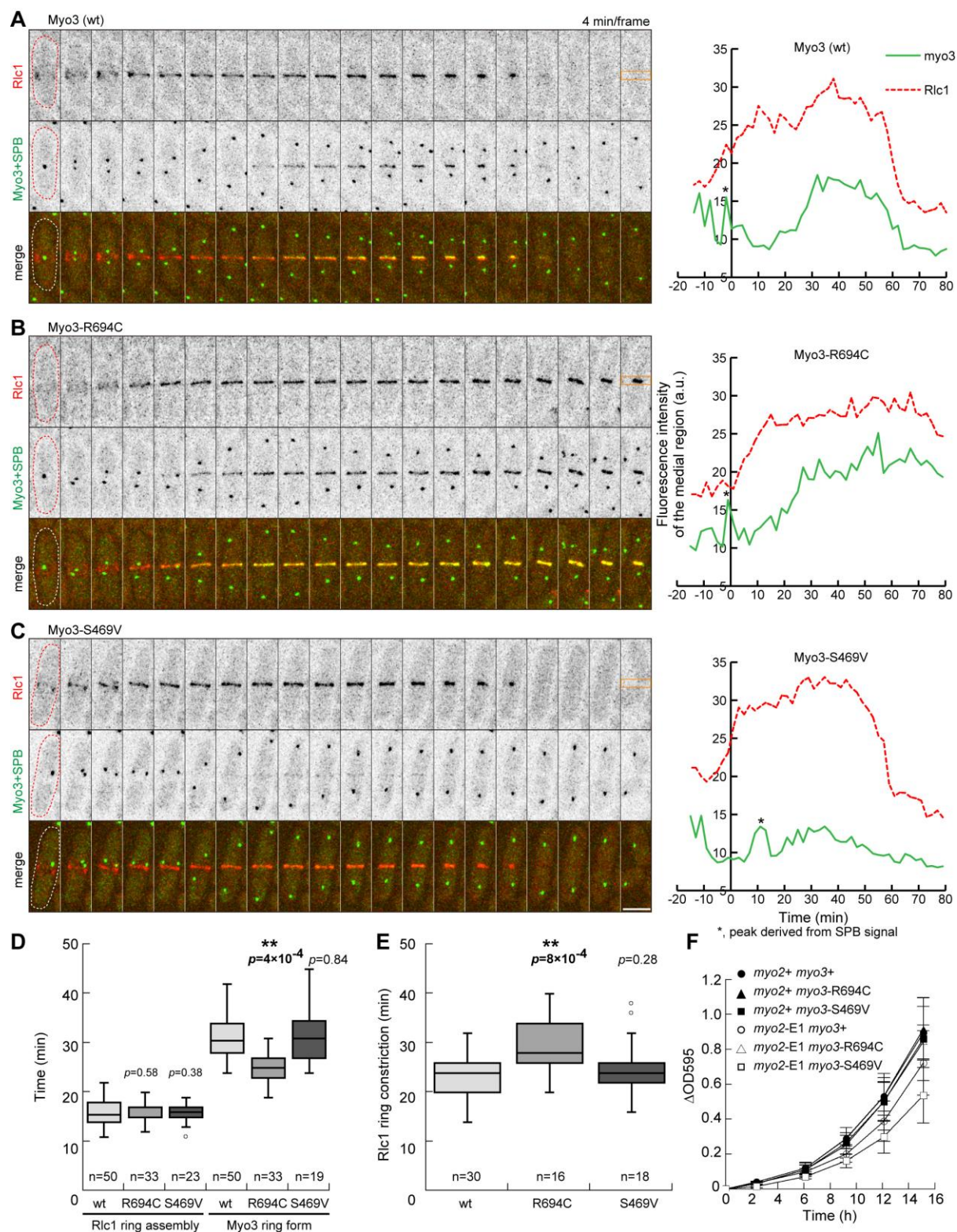


**Fig. 3. Localization and functions of mutant Myo3s**

(A) Positions of the point-mutations introduced into Myo3 were indicated on the structure of *Dictyostelium* myosin-II head (PDB code: 1MMG) drawn by Jmol. (B) Summary of the functions and local concentrations of the mutant Myo3s, and characteristics of the original

point-mutations (see also Fig. S1). (C) A Western blot analysis of the protein levels of wt and mutant Myo3s. Myo3-3mYFP was detected as a 320-kd band by an anti-GFP antibody. The levels of  $\alpha$ -tubulin were shown as a loading control. (D) Localization of wt and mutant Myo3s in late anaphase cells. (E) Dot plot of fluorescence intensities of the mutant Myo3-3mYFP rings (*see Methods*). Data were pooled from three independent experiments. Horizontal lines indicate the means. Double asterisks indicate a significant difference (vs. wt,  $p < 0.01$ ). (F) Cells expressing Myo3-G688V-3mYFP and Sid4-3mCherry were imaged. (G) The localization of Myo3 and the Myo3 tail expressed under the control of the *nmt41* promotor. Cells were grown in the presence of 5  $\mu$ M thiamine and then imaged in a single focal plane. (H) Cells expressing wt and mutant Myo3s were grown in the presence of 1 M KCl. Bars, 5  $\mu$ m.



medial region (a boxed region) were plotted over time. (D-E) Box plots of times required for the assembly of Rlc1 and mutant Myo3 rings from the SPB separation. (E) Box plot of the time required for constriction of the Rlc1 ring. Data in (D-E) were pooled from two independent preparations. Double asterisks indicate a significant difference (vs. wt,  $p < 0.01$ ). (F) Growth curves of wt and mutant *myo3-3mYFP* cells cultivated at 25°C. Data are the mean  $\pm$  SD (error bars) from three independent measurements. Bars, 5  $\mu\text{m}$ .

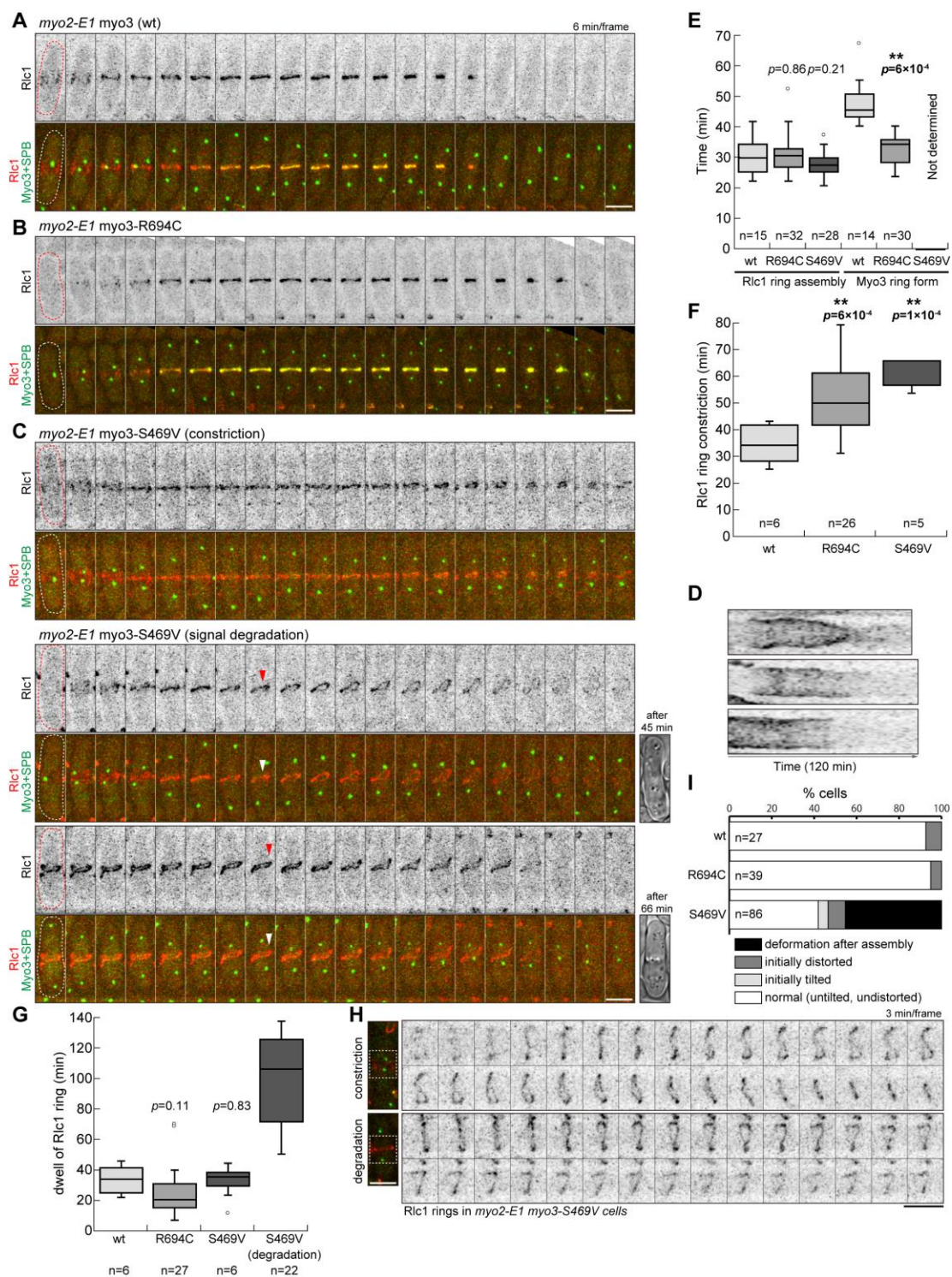


**Fig. 5. Sufficient accumulation of Myo3 to the CR was required for its maintenance in the *myo2-E1* background**

(A-C) Simultaneous observation of Rlc1 and Myo3 (A), Myo3-R694C (B), or Myo3-S469V (C) during assembly and constriction of the CR in the *myo2-E1* background. Arrowheads

indicate the onset of ring deformation. (D) Kymographs of the Rlc1 rings shown in (C). (E) Box plots of times required for the assembly of Rlc1 and mutant Myo3 rings from the SPB separation. (F) Box plot of the time required for constriction of the Rlc1 ring. (G) Box plot of the duration of unconstricted rings. (H) Deformation of Rlc1 rings in *myo2-E1 myo3-S469V* cells. Boxed regions of the cells were magnified 1.5 times. (I) The rings in the cells of indicated genotypes were scored according to their deformation. Data in (E-G, I) were pooled from 2–4 independent experiments. Double asterisks indicate a significant difference (vs. wt,  $p < 0.01$ ). Bars, 5  $\mu\text{m}$ .

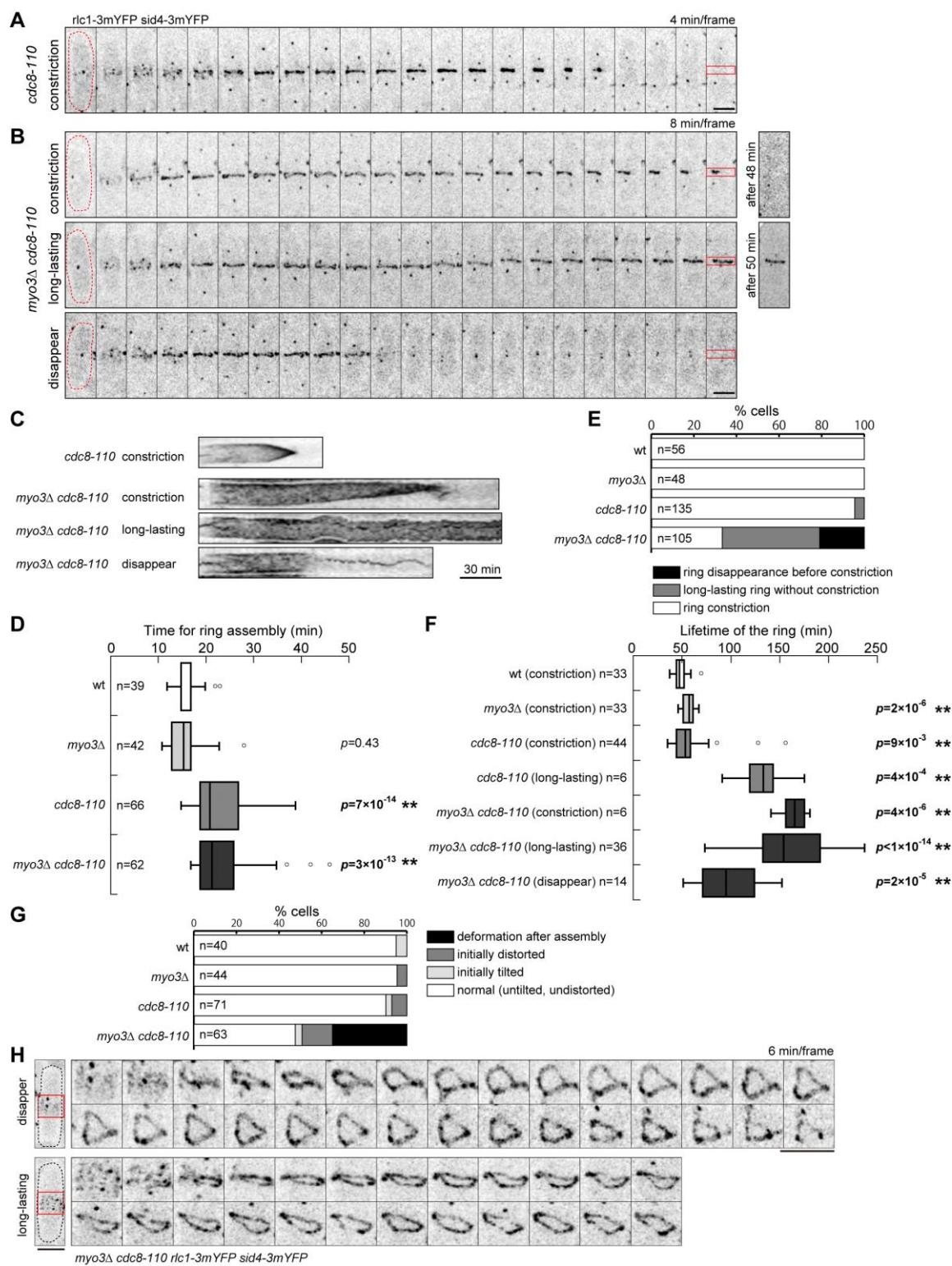


**Fig. 6. Synthetic genetic interaction between *myo3* and *cdc8***

(A-B) Time-lapse imaging of the assembly and constriction of Rlc1 rings in *cdc8-110* (A) and *myo3Δ cdc8-110* (B) cells. (C) Kymographs of the boxed regions shown in (A-B). (D)

Box plot of the times required for the assembly of Rlc1 from the SPB separation. (E) The Rlc1 rings in the cells of the indicated genotypes were scored according to their behaviors. (F) Box plot of the lifetime of the Rlc1 ring from its assembly to the disappearance of its signal. (G) Rlc1 rings were scored according to their deformation. Data in (D-G) were pooled from 2-5 independent experiments. (H) Deformation of the rings in *myo3Δ cdc8-110* cells. Boxed regions of the cells were magnified two times. Double asterisks indicate a significant difference (vs. wt,  $p < 0.01$ ). Bars, 5  $\mu\text{m}$ .

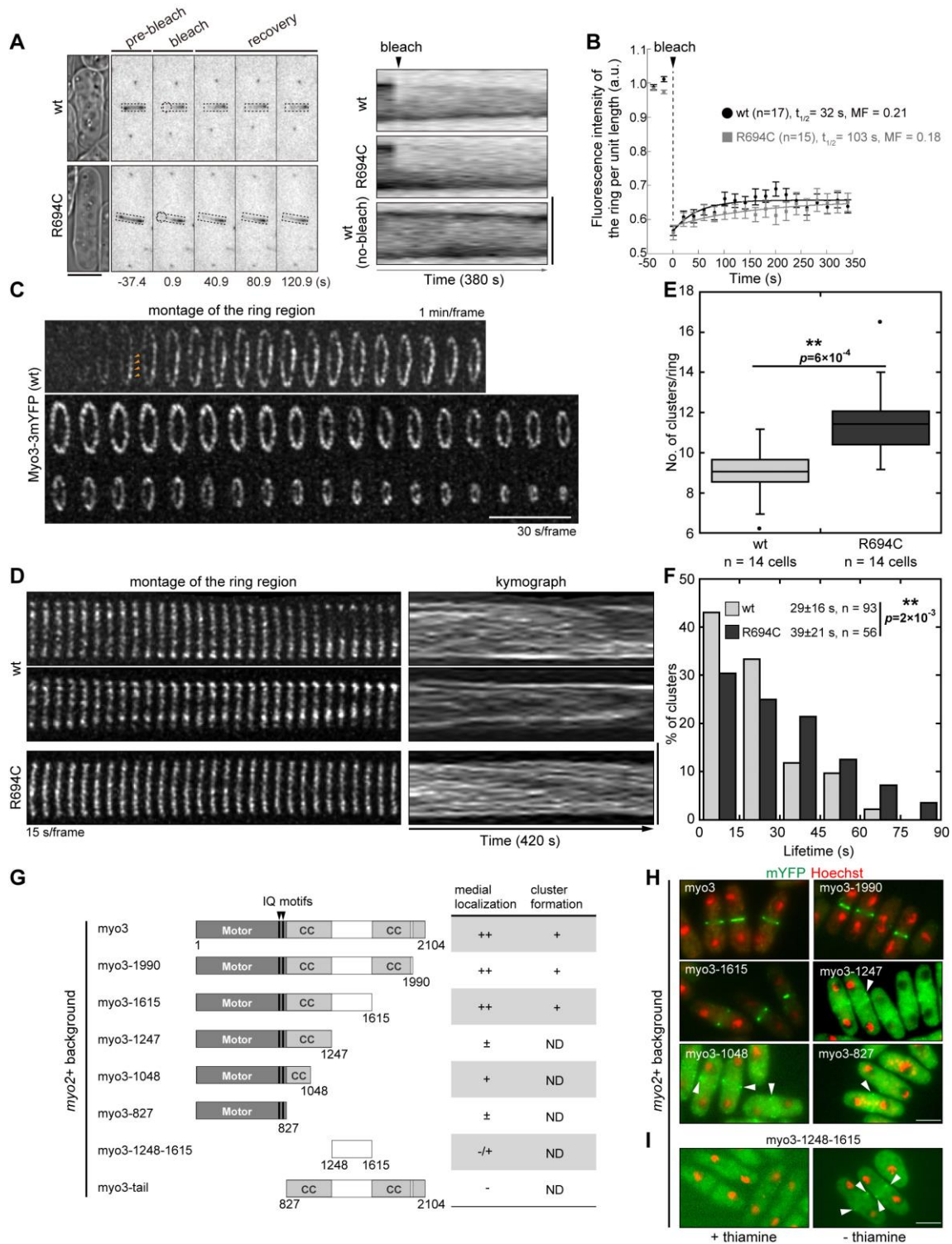


**Fig. 7. Myo3 formed motile clusters on the ring**

(A) The ring of Myo3-3mYFP or Myo3-R694C-3mYFP (boxed regions) was photobleached at  $t = 0$  s on one side (in a circle) and imaged. *Right*, kymographs of the boxed region. (B)

The fluorescence intensities of bleached regions were plotted over time. Data are the mean plotted over time. Data are the mean  $\pm$  SEM (error bars). Best fit curves were drawn. (C) Slightly tilted *myo3-3mYFP sid4-3mYFP* cells were imaged. Maximum projections of *z*-stacked deconvolved images. Arrowheads indicate the emergence of Myo3 clusters. (D) Clusters of Myo3 and Myo3-R694C were examined by time-lapse imaging (*see Methods*). *Right*, kymographs of the ring region. (E) Box plot of the time-averaged number of Myo3 clusters detected per ring (*see Methods*). Data were pooled from four independent experiments. (F) The lifetime distribution of individual clusters. Data were pooled from 3–4 independent experiments. The mean  $\pm$  SD is shown. (G) Diagram of the *myo3* deletion forms. The localization of the mutant proteins in *myo2*<sup>+</sup> strains was summarized. Note that all these mutant forms were expressed from the original locus in place of the endogenous Myo3. (H) Cells expressing the indicated forms of Myo3-3mYFP were imaged in a single focal plane. (I) Myo3-1245-1615-3mYFP was expressed under the control of the *nmt41* promoter in the presence or absence of thiamine for 19–25h. Arrowheads in (H-I) indicate the medial localization of mutant *myo3*s. Double asterisks indicate a significant difference ( $p < 0.01$ ). Bars, 5  $\mu$ m.

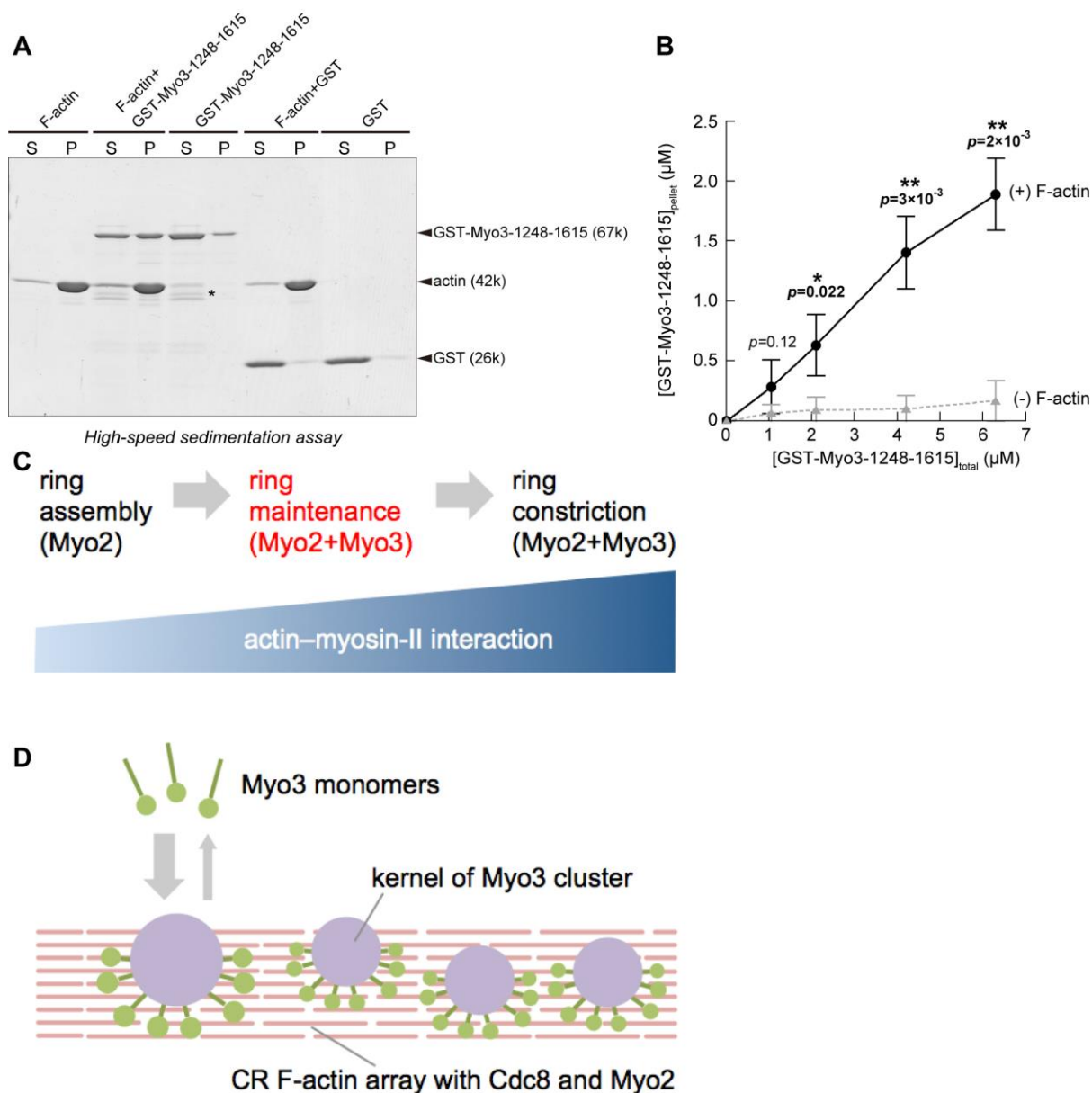


**Fig. 8. Models for the function of the actin–myosin-II interaction and Myo3 during cytokinesis**

(A) Sedimentation of GST, GST-Myo3-1248-1615, and F-actin. Samples were centrifuged, and the supernatant (S) and pellet (P) fractions were analyzed by SDS-PAGE. An asterisk indicates degradation products. (B) F-actin increased the amount of sedimentable Myo3-1248-1615. Several concentrations of GST-Myo3-1248-1615 were centrifuged in the absence and presence of F-actin, and the bands in the pellet fraction were quantified. Data are the

mean  $\pm$  SD (error bars) of three independent experiments. Asterisks indicate a significant difference versus (-) F-actin. (C) Most Myo3 joined the CR after its assembly, augmenting the net actin–myosin-II interaction in the ring. Myo3 and Myo2 maintained and then constricted the ring. Cdc8 enhanced the actin–myosin-II interaction (not depicted). (D) A model for the localization and function of Myo3.

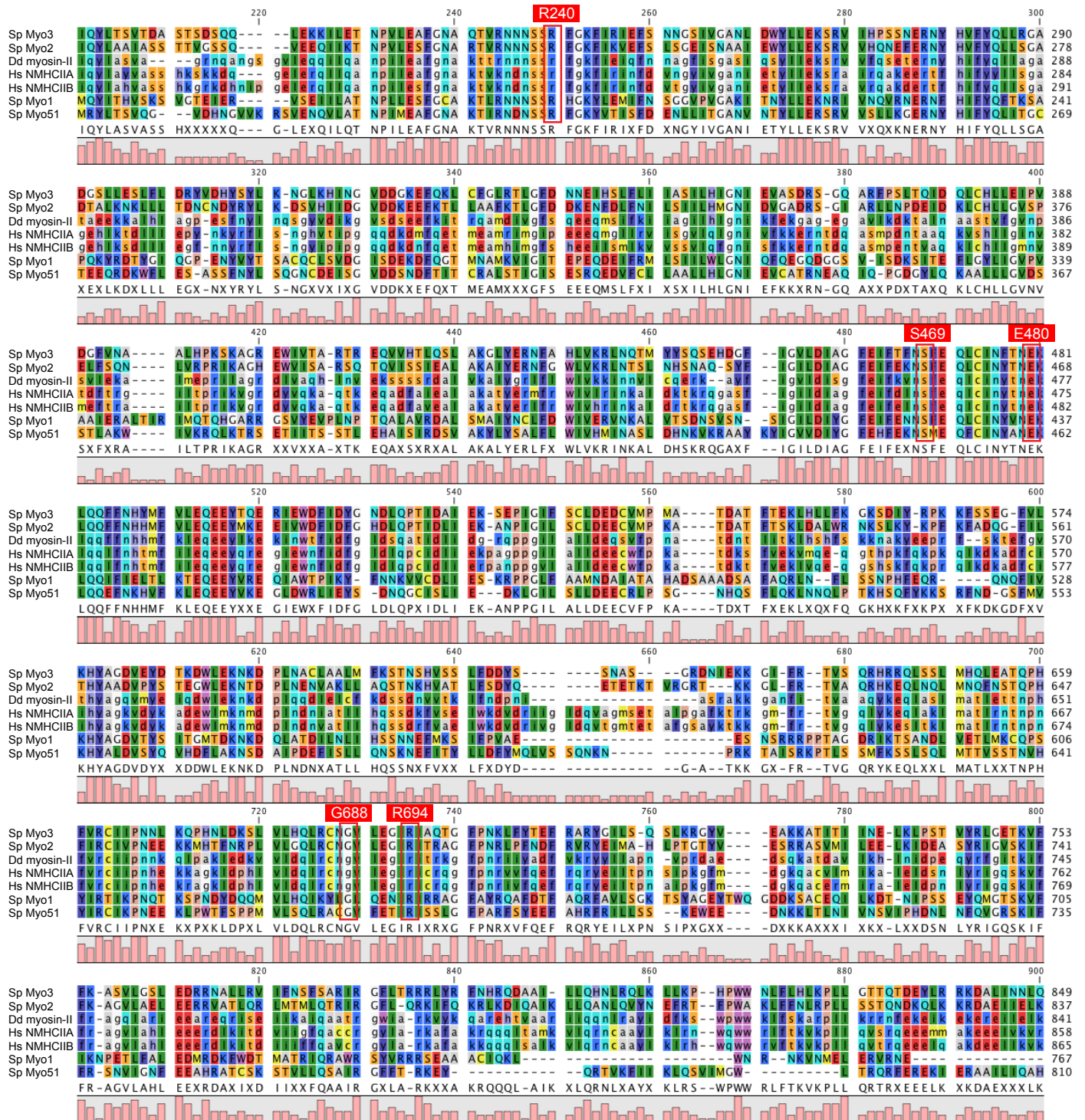


Fig. S1 Point-mutations introduced into Myo3

The deduced amino acid sequence of *S. pombe* Myo3 (Sp Myo3; GenBank accession no. AAC04615) was aligned with *S. pombe* Myo2 (Sp Myo2; AAC49908), the *D. discoideum* myosin-II heavy chain (Dd myosin-II; EAL64202), *H. sapiens* non-muscle myosin-IIA (MYH9) (Hs NMHCIIA; EAW60098), *H. sapiens* non-muscle myosin-IIB (MYH10) (Hs NMHCIIIB; AAI17692), *S. pombe* Myo1 (type-I myosin) (Sp Myo1; CAB46766), and *S. pombe* Myo51 (type-V myosin) (Sp Myo51; CAA21172) by CLC Sequence Viewer 7. A part of the alignment (around residues 200-800) was shown. Boxed regions indicate conserved residues into which the mutations were introduced.

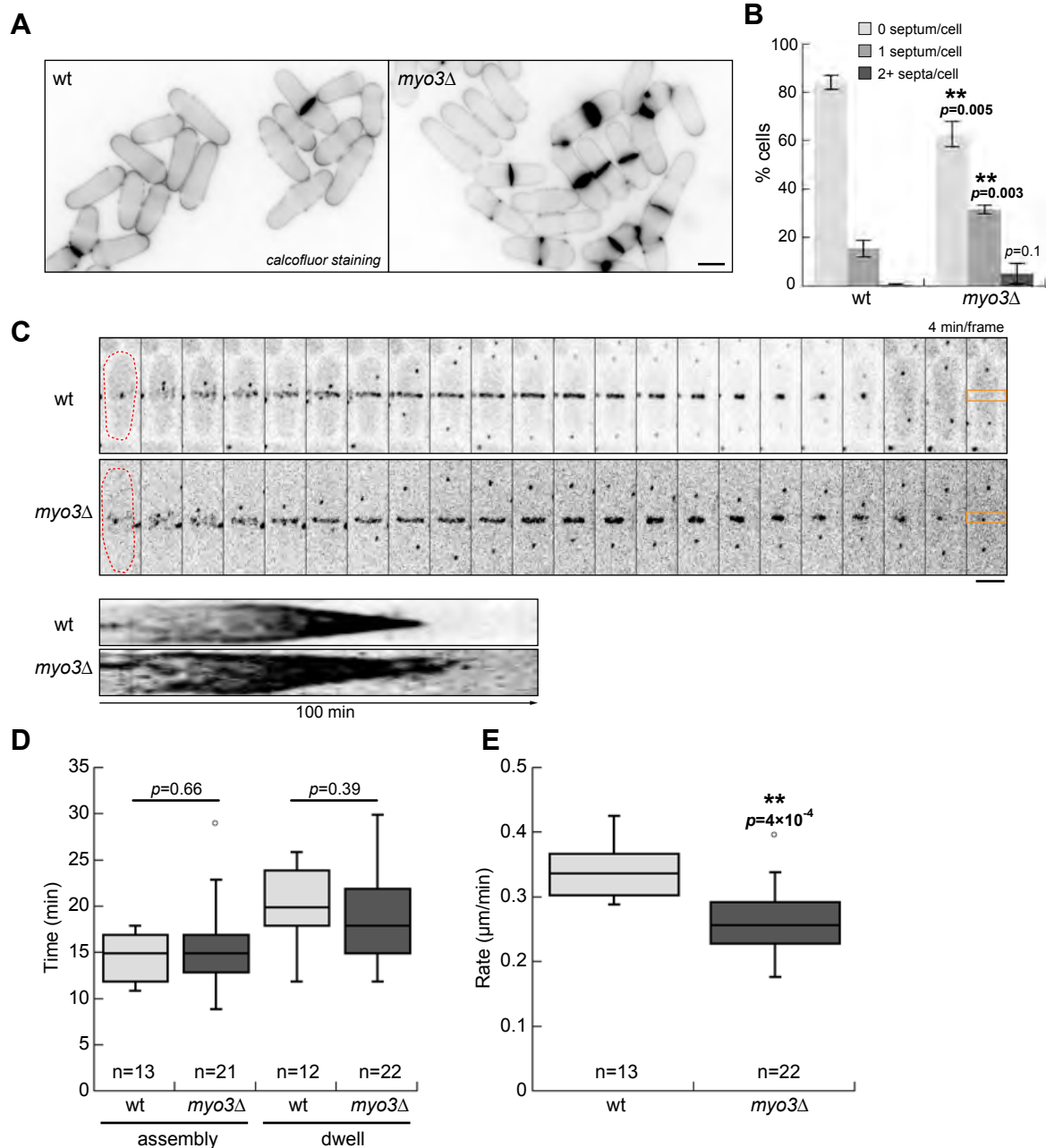


Fig. S2 Deletion of *myo3+* reduced the constriction rate of the CR and septation efficiency (A) Septa of wt and *myo3Δ* cells grown at 30°C were stained and imaged. (B) Quantification of the number of septa per cell. Data are the mean  $\pm$  SD (error bars) from three independent experiments (300-700 cells were scored at each measurement). (C) Time-lapse imaging of the assembly and constriction of Rlc1 rings in wt and *myo3Δ* cells. Bottom, kymographs of the boxed regions. (D) Box plots of the time required for the assembly of Rlc1 rings from the SPB separation and time of the dwell phase. (E) Box plot of the rate of Rlc1 ring constriction. Data in (D-E) were pooled from two independent experiments. Double asterisks indicate a significant difference ( $p < 0.01$ ). Bars, 5  $\mu\text{m}$ .

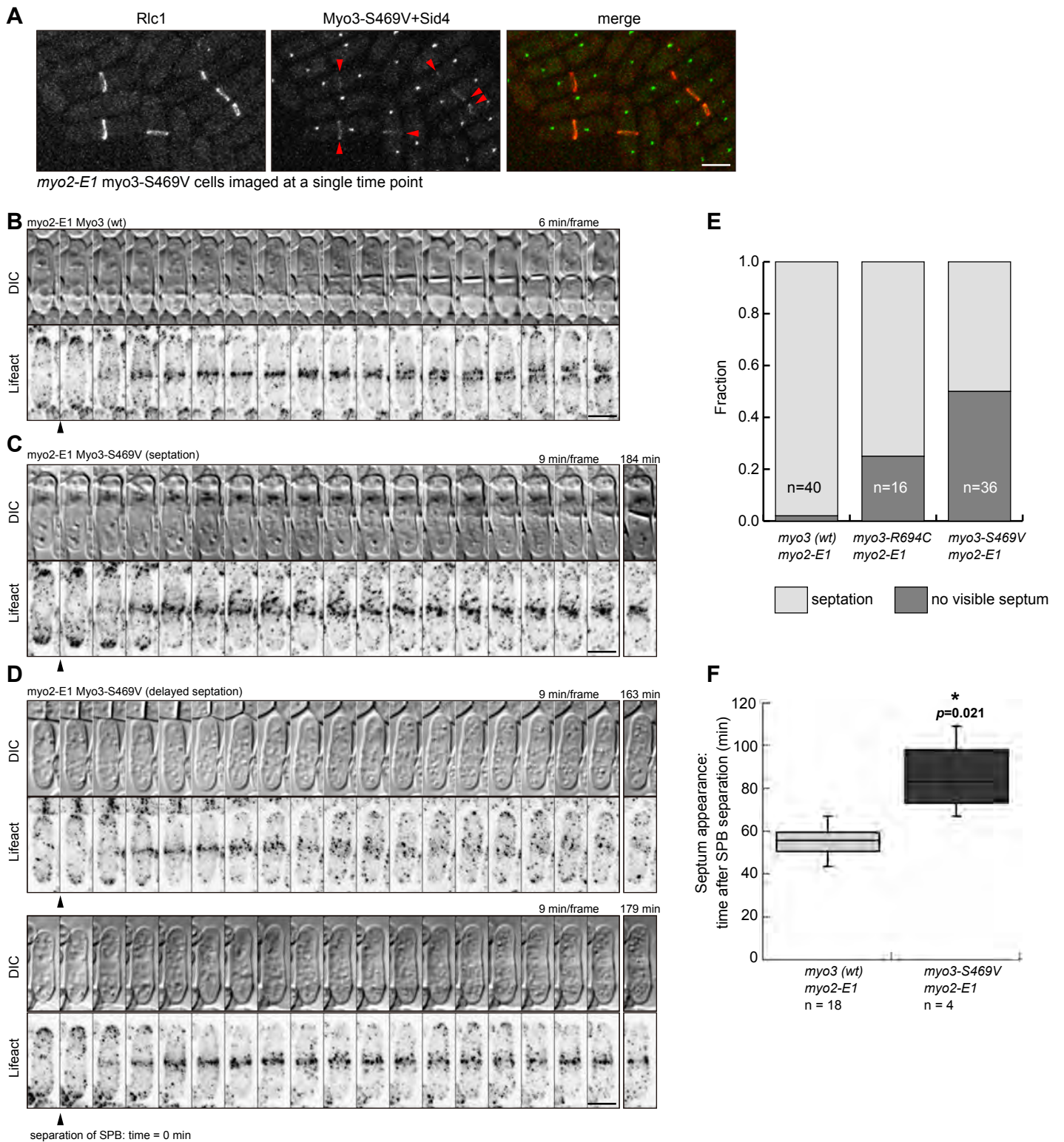


Fig. S3 Behavior of the medial actin ring in *myo2-E1 myo3-S469V* cells

(A) A stack of z-sections of *myo2-E1 rlc1-3mCherry myo3-S469V-3mYFP sid4-3mYFP* cells was acquired at a single time point using a confocal microscope (LSM 700; Carl Zeiss, Inc.). The experimental conditions were the same as those used in Figure 5, except that cells were not repeatedly scanned by lasers. Arrowheads indicate Myo3-S469V-3mYFP localizing to the CR in the *myo2-E1* background. (B-D) Observation of the medial actin ring during cytokinesis in cells expressing Myo3-3mYFP (B) or Myo3-S469V (C, D) in the *myo2-E1* background. Arrowheads indicate the timing of the SPB separation. (E) The cells of the indicated genotypes were scored according to septum formation in bright field images. These cells were observed for at least 70 (wt) or 95 (R694C and S469V) min after the SPB separation. (F) Box plot of the time from SPB separation to the appearance of a visible septum. An asterisk indicates a significant difference (vs. wt,  $p < 0.05$ ). Data in (E-F) were pooled from two independent experiments. Bars, 5  $\mu$ m.

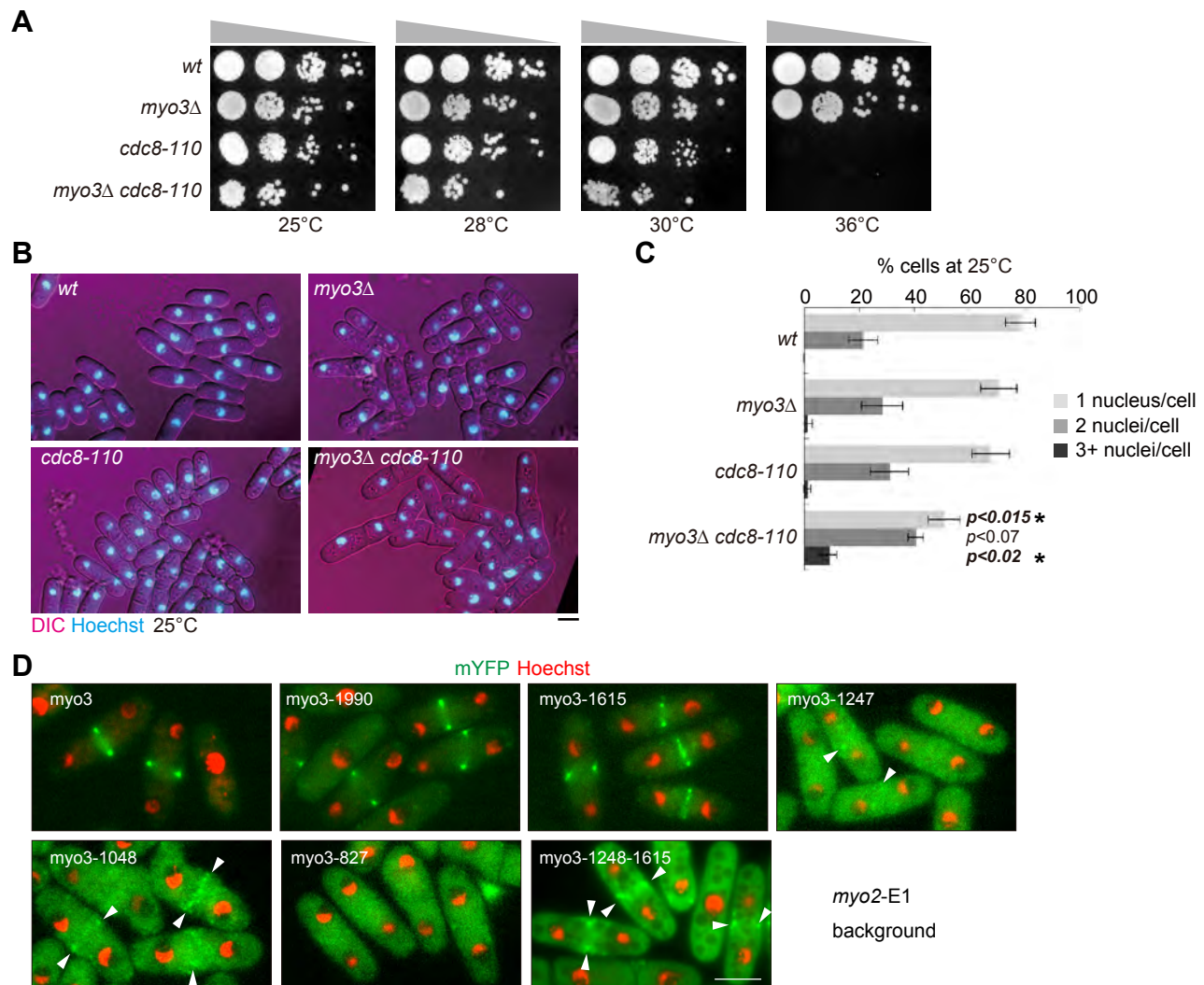


Fig. S4 Genetic interaction between *myo3Δ* and *cdc8-110*, and localization of the *myo3* deletion forms in the *myo2-E1* background

(A) Cells of the indicated genotypes were serially diluted, spotted on plates, and grown for 3 days at the indicated temperature. (B) Cells were grown at 25°C, stained with Hoechst, and then imaged in a single focal plane. (C) Quantification of the number of nuclei per cell. Data are the mean  $\pm$  SD (error bars) from three independent experiments (250–500 cells were scored at each measurement). P-values were calculated versus the three other strains, and the most stringent conditions were shown. Asterisks indicate a significant difference ( $p < 0.05$ ). (D) Localization of the *myo3* deletion forms in the *myo2-E1* background. Cells expressing the indicated forms of Myo3-3mYFP were imaged in a single focal plane. Myo3-1245–1615-3mYFP was expressed under the control of the *nmt41* promoter in the absence of thiamine for 36 h. Arrowheads indicate the medial localization of mutant *myo3*s. Bars, 5  $\mu$ m.

**Table S1. Strains used in this study**

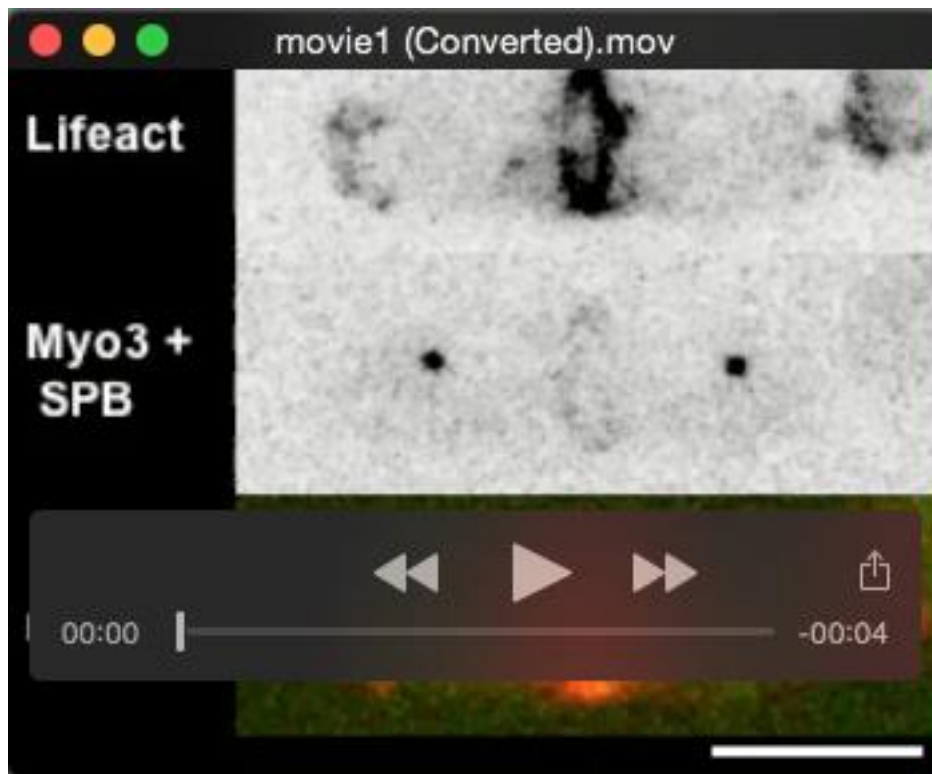
| Name    | Genotype                                                                          | Source     | Figure   |
|---------|-----------------------------------------------------------------------------------|------------|----------|
| MTY672  | myo3 $\Delta$ head::ura4 (delete 0.4-2.4kbp)-3mYFP-3HA:hphMX6                     | This study |          |
| MTY616  | mYFP-Myo2 Pcde4-lifeact-4mCherry sid4-3mYFP-3HA:hph                               | Lab stock  | 1        |
| MTY597  | myo3-3mYFP-3HA:hph sid4-3mYFP-3HA:kan Pcde4-lifeact-4mCherry                      | This study | 1, 2     |
| MTY904  | mid1 $\Delta$ ::ura4 myo3-3mYFP-3HA:hph sid4-3mYFP-3HA:kan Pcde4-lifeact-4mCherry | This study | 2        |
| MTY1020 | myo3-G688V-3mYFP-3HA-hphMX6 sid4-4mCherry:kanMX6                                  | This study | 3        |
| MTY465  | myo3-3mYFP-3HA:hphMX6                                                             | This study | 3        |
| MTY473  | myo3-S469V-3mYFP-3HA:hphMX6                                                       | This study | 3        |
| MTY474  | myo3-R694C-3mYFP-3HA:hphMX6                                                       | This study | 3        |
| MTY497  | myo3-E480K-3mYFP-3HA:hphMX6                                                       | This study | 3        |
| MTY498  | myo3-R240A-3mYFP-3HA:hphMX6                                                       | This study | 3        |
| MTY642  | kan:Pnmt41-myo3-3mYFP-3HA:hph                                                     | This study | 3        |
| MTY685  | myo3-G688V-3mYFP-3HA:hphMX6                                                       | This study | 3        |
| MTY693  | myo3-G688V-3mYFP-3HA rlc1-3mCherry sid4-3mYFP-3HA                                 | This study | 3        |
| MTY716  | myo3-E480K-3mYFP-3HA sid4-3mYFP-3HA                                               | This study | 3        |
| MTY718  | myo3-R240A-3mYFP-3HA sid4-3mYFP-3HA:kan                                           | This study | 3        |
| MTY719  | myo3-G688V-3mYFP-3HA sid4-3mYFP-3HA                                               | This study | 3        |
| MTY724  | myo3-S469V-3mYFP-3HA sid4-3mYFP-3HA:kan                                           | This study | 3        |
| MTY528  | myo3-3mYFP-3HA:hphMX6 sid4-3mYFP-3HA:kan                                          | This study | 3, 7     |
| MTY569  | kan:Pnmt41-myo3tail-3mYFP-3HA:hphMX6                                              | This study | 3, 7     |
| MTY717  | myo3-R694C-3mYFP-3HA sid4-3mYFP-3HA:kan                                           | This study | 3, 7     |
| MTY551  | myo3-3mYFP-3HA:hphMX6 rlc1-3mCherry sid4-3mYFP-3HA                                | This study | 4        |
| MTY704  | myo3-S469V-3mYFP-3HA rlc1-3mCherry sid4-3mYFP-3HA                                 | This study | 4        |
| MTY913  | myo3-R694C-3mYFP-3HA rlc1-3mCherry sid4-3mYFP-3HA                                 | This study | 4        |
| MTY636  | rlc1-3mYFP-3HA sid4-3mYFP-3HA:kan                                                 | Lab stock  | 6, S2    |
| MTY684  | myo3 $\Delta$ :kan rlc1-3mYFP-3HA sid4-3mYFP-3HA:kan                              | This study | 6, S2    |
| MTY777  | myo2-E1 myo3-3mYFP-3HA rlc1-3mCherry sid4-3mYFP-3HA                               | This study | 4, 5     |
| MTY778  | myo2-E1 myo3-R694C-3mYFP-3HA rlc1-3mCherry sid4-3mYFP-3HA                         | This study | 4, 5     |
| MTY780  | myo2-E1 myo3-S469V-3mYFP-3HA rlc1-3mCherry sid4-3mYFP-3HA                         | This study | 4, 5, S3 |
| MTY982  | cde8-110 rlc1-3mYFP-hphMX6 sid4-3mYFP-3HA                                         | This study | 6        |
| MTY983  | cde8-110 myo3 $\Delta$ ::kan rlc1-3mYFP-hphMX6 sid4-3mYFP-3HA                     | This study | 6        |

|         |                                                                         |            |    |
|---------|-------------------------------------------------------------------------|------------|----|
| MTY1001 | myo3-1990-3mYFP-3HA:hphMX6                                              | This study | 7  |
| MTY1002 | myo3-1615-3mYFP-3HA:hphMX6                                              | This study | 7  |
| MTY1003 | myo3-1247-3mYFP-3HA:hphMX6                                              | This study | 7  |
| MTY1004 | myo3-827-3mYFP-3HA:hphMX6                                               | This study | 7  |
| MTY1008 | myo3-1048-3mYFP-3HA:hphMX6                                              | This study | 7  |
| MTY1010 | kanMX6:Pnmt41-myo3-1248-1615-3mYFP:hphMX6                               | This study | 7  |
| MTY838  | myo2-E1 myo3-3mYFP-3HA:hph sid4-3mYFP-3HA:kan Pcdc4-lifeact-4mCherry    | This study | S3 |
| MTY839  | myo2-E1 myo3-S469V-3mYFP-3HA sid4-3mYFP-3HA Pcdc4-lifeact-4mCherry:ura4 | This study | S3 |
| MTY840  | myo2-E1 myo3-R694C-3mYFP-3HA sid4-3mYFP-3HA Pcdc4-lifeact-4mCherry:ura4 | This study | S3 |
| MTY10   | ura4D-18 leu1-32                                                        | Lab stock  | S4 |
| MTY16   | cdc8-110                                                                | Lab stock  | S4 |
| MTY78   | myo3Δ::kanMX6                                                           | This study | S4 |
| MTY88   | myo3Δ::kanMX6 cdc8-110                                                  | This study | S4 |
| MTY1078 | myo2-E1 myo3-3mYFP-3HA:hphMX6                                           | This study | S4 |
| MTY1079 | myo2-E1 myo3-1990-3mYFP-3HA:hphMX6                                      | This study | S4 |
| MTY1080 | myo2-E1 myo3-1615-3mYFP-3HA:hphMX6                                      | This study | S4 |
| MTY1081 | myo2-E1 myo3-1247-3mYFP-3HA:hphMX6                                      | This study | S4 |
| MTY1082 | myo2-E1 myo3-1048-3mYFP-3HA:hphMX6                                      | This study | S4 |
| MTY1083 | myo2-E1 myo3-827-3mYFP-3HA:hphMX6                                       | This study | S4 |
| MTY1084 | myo2-E1 kanMX6:Pnmt41-myo3-1248-1615-3mYFP:hphMX6                       | This study | S4 |

**Table S2. Plasmids used in this study**

| Name   | Structure             | Source     | Purpose |
|--------|-----------------------|------------|---------|
| MTP467 | pREP81-GFP-myo3       | Lab stock  |         |
| MTP461 | pREP81-GFP-myo3-R240A | This study | MTY498  |
| MTP465 | pREP81-GFP-myo3-G688V | This study | MTY685  |
| MTP466 | pREP81-GFP-myo3-E480K | This study | MTY497  |
| MTP486 | pREP81-GFP-myo3-S469V | This study | MTY473  |
| MTP487 | pREP81-GFP-myo3-R694C | This study | MTY474  |

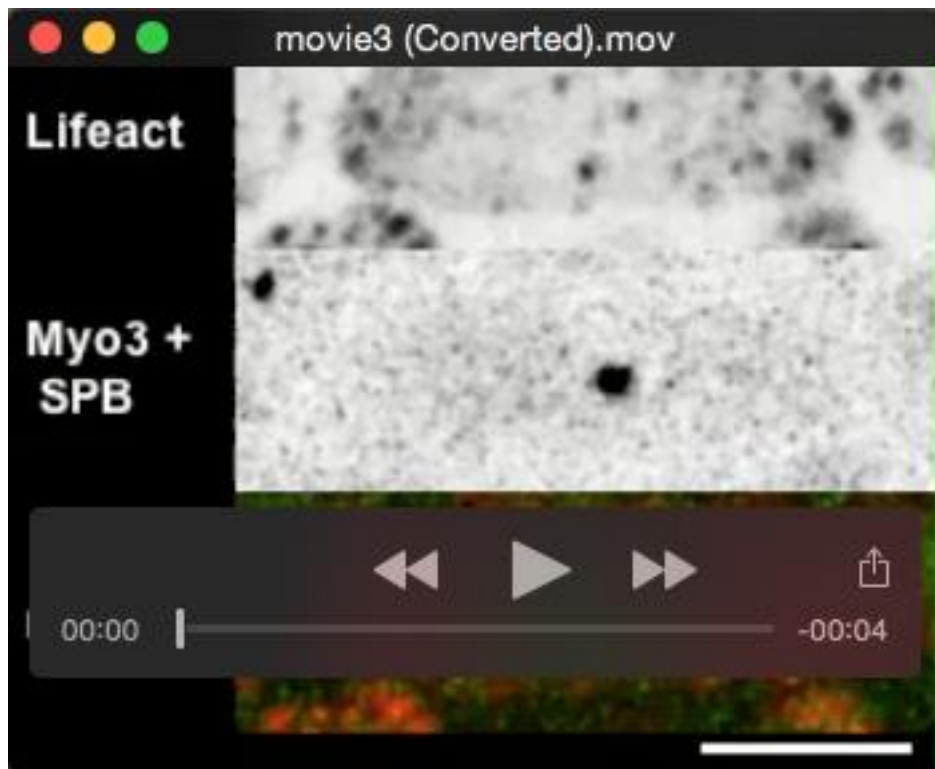
## Movies



**Movie 1. Myo3 and actin rings in DMSO-treated cells.** Related to Figure 1C. Strain: MTY597 (*myo3-3mYFP sid4-3mYFP Pcdc4-lifeact-4mCherry*). Time-lapse imaging of Myo3-3mYFP and actin rings using an inverted fluorescence microscope (BX71; Olympus) equipped with a UPlanSApo 100 $\times$ /1.40 NA objective lens (Olympus), spinning-disk confocal scanner (CSU22; Yokogawa), piezo objective positioner (E-665; Physik Instrumente), electron multiplying CCD camera (iXon 3 885; Andor), and emission beam splitter (Dual View; Roper Scientific) with excitation by 488-nm and 568-nm lasers using GFP and mCherry filters and MetaMorph software (version 7.7.5.0; Molecular Devices). Myo3, Lifeact, and SPBs in late anaphase cells were simultaneously imaged at 1-min intervals. A total of 0.36% DMSO was supplemented at  $t = 00:00$ . Stacks of 12 confocal  $z$ -sections spaced by 0.45  $\mu\text{m}$  were collected every minute for 30 min, and projected to an  $xy$  image using a maximum intensity projection. Green, Myo3-3mYFP and Sid4-3mYFP; red, Lifeact-4mCherry. Bar, 5  $\mu\text{m}$ .



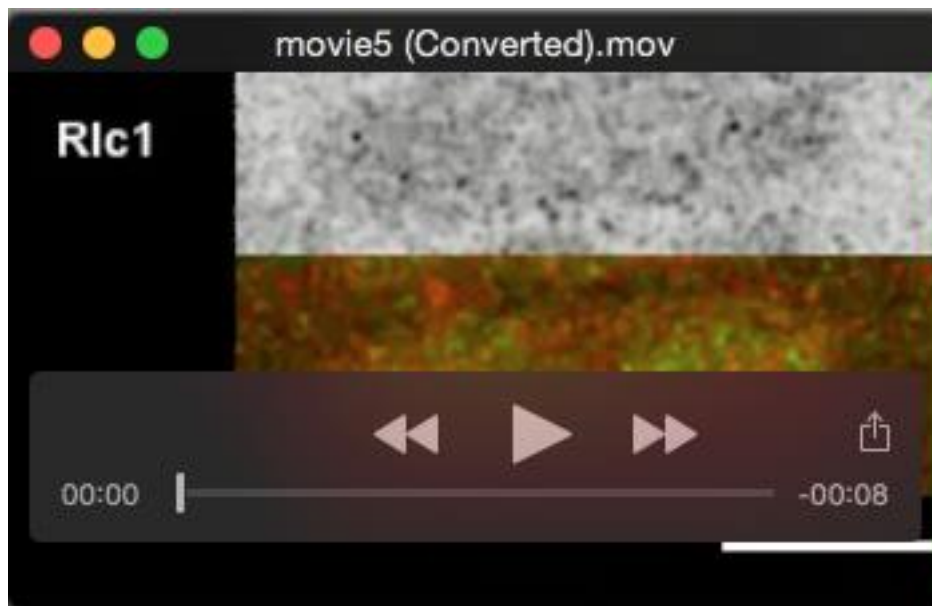
**Movie 2. Myo3 and actin rings in Lat-A-treated cells.** Related to Figure 1D. Strain: MTY597 (*myo3-3mYFP sid4-3mYFP Pcdc4-lifeact-4mCherry*). Time-lapse imaging of Myo3-3mYFP and actin rings using an inverted fluorescence microscope (BX71; Olympus) equipped with a UPlanSApo 100 $\times$ /1.40 NA objective lens (Olympus), spinning-disk confocal scanner (CSU22; Yokogawa), piezo objective positioner (E-665; Physik Instrumente), electron multiplying CCD camera (iXon 3 885; Andor), and emission beam splitter (Dual View; Roper Scientific) with excitation by 488-nm and 568-nm lasers using GFP and mCherry filters and MetaMorph software (version 7.7.5.0; Molecular Devices). Myo3, Lifeact, and SPBs in late anaphase cells were simultaneously imaged at 1-min intervals. A total of 0.36% DMSO plus 7  $\mu$ M Lat-A was supplemented at  $t = 00:00$ . Stacks of 12 confocal  $z$ -sections spaced by 0.45  $\mu$ m were collected every minute for 30 min, and projected to an  $xy$  image using a maximum intensity projection. Green, Myo3-3mYFP and Sid4-3mYFP; red, Lifeact-4mCherry. Bar, 5  $\mu$ m.



**Movie 3. Assembly of Myo3 and actin rings.** Related to Figure 2A. Strain: MTY597 (*myo3-3mYFP sid4-3mYFP Pcdc4-lifeact-4mCherry*). Time-lapse imaging of Myo3-3mYFP and actin rings using a confocal microscope (LSM 700; Carl Zeiss, Inc.) equipped with an alpha Plan-Apochromat 100×/1.46 NA objective lens (Carl Zeiss, Inc.). The duplicated SPBs separated at  $t = 00:00$ . Stacks of 12 confocal z-sections spaced by  $0.62 \mu\text{m}$  were collected every 2 minutes for 60 min, and projected to an  $xy$  image using a maximum intensity projection. Green, Myo3-3mYFP and Sid4-3mYFP; red, Lifeact-4mCherry. Bar,  $5 \mu\text{m}$ .



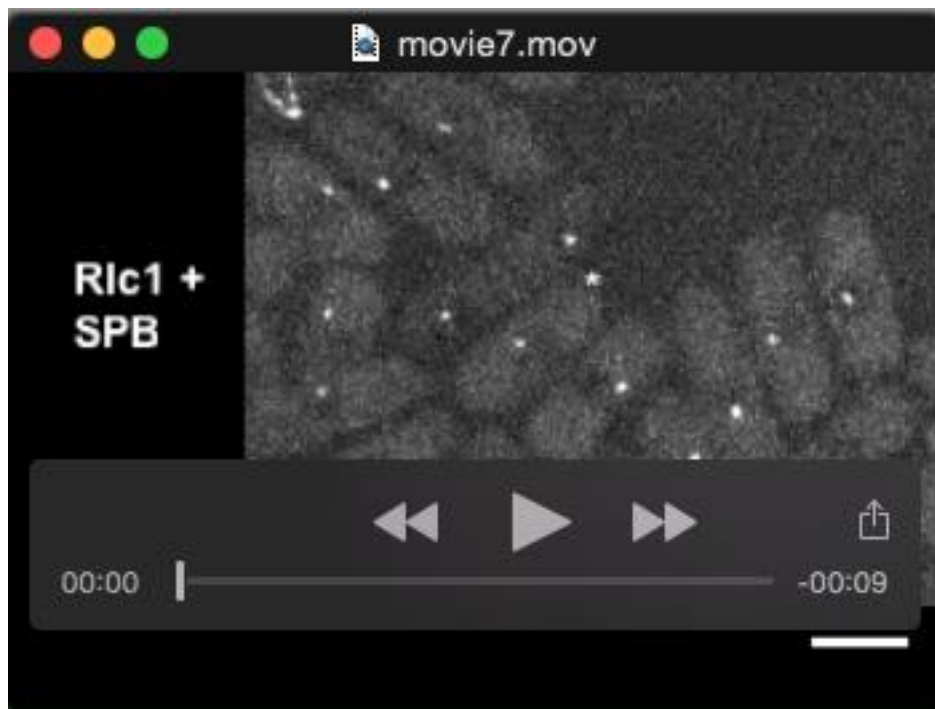
**Movie 4. Assembly of Myo3 and Rlc1 rings.** Related to Figures 4A-B. Strains: MTY551 (*myo3-3mYFP rlc1-3mCherry sid4-3mYFP*) (left column) and MTY913 (*myo3-R694C-3mYFP rlc1-3mCherry sid4-3mYFP*) (right column). Time-lapse imaging of Myo3 and Rlc1 rings using a confocal microscope (LSM 700; Carl Zeiss, Inc.) equipped with an alpha Plan-Apochromat 100×/1.46 NA objective lens (Carl Zeiss, Inc.). The duplicated SPBs separated at  $t = 00:00$ . Stacks of 13 confocal  $z$ -sections spaced by  $0.62 \mu\text{m}$  were collected every 2 minutes for 90 min, and projected to an  $xy$  image using a maximum intensity projection. Green, Myo3-3mYFP and Sid4-3mYFP; red, Rlc1-3mCherry. Bar,  $5 \mu\text{m}$ .



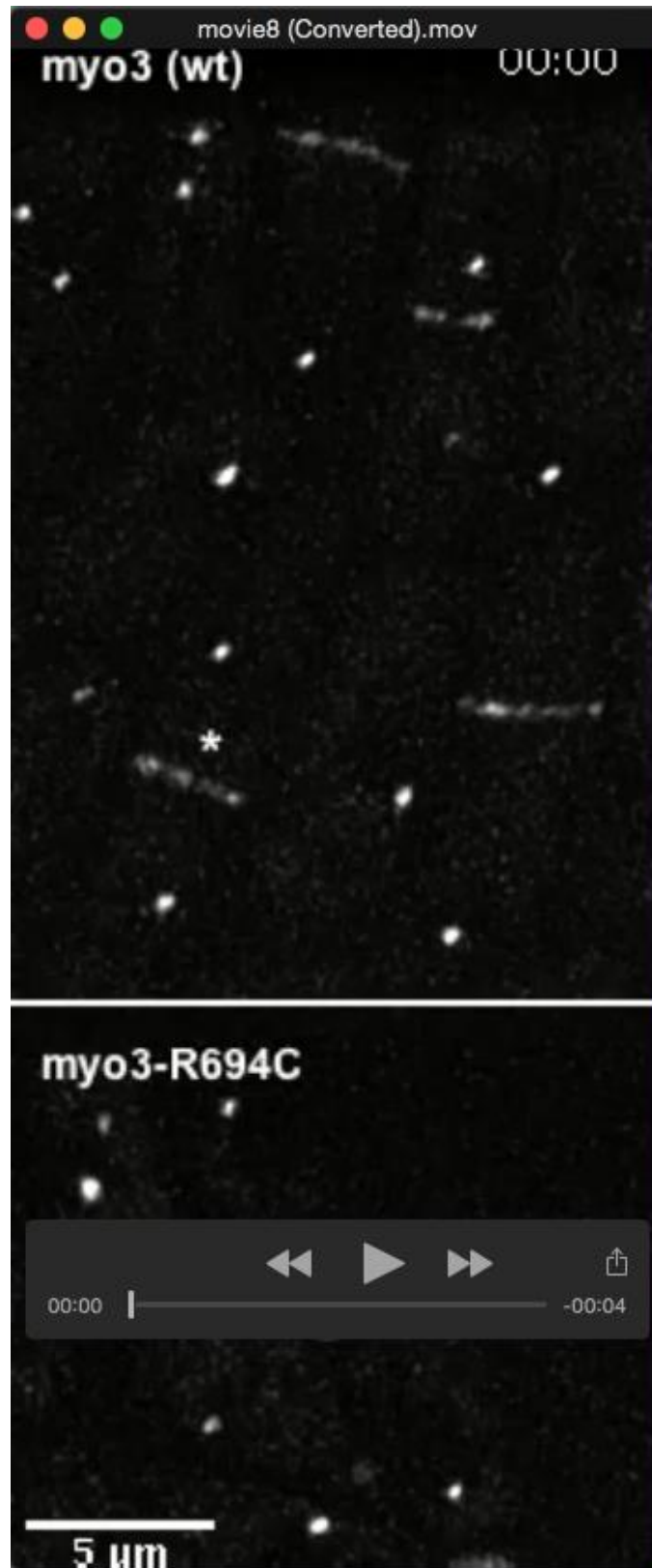
**Movie 5. Constriction of the Rlc1 ring in the *myo2-E1 myo3-S469V* background.** Related to the upper panel of Figure 5C. Strain: MTY780 (*myo2-E1 myo3-S469V-3mYFP rlc1-3mCherry sid4-3mYFP*). Time-lapse imaging of Myo3-S469V and Rlc1 rings using a confocal microscope (LSM 700; Carl Zeiss, Inc.) equipped with an alpha Plan-Apochromat 100 $\times$ /1.46 NA objective lens (Carl Zeiss, Inc.). The duplicated SPBs separated at  $t = 00:00$ . Stacks of 13 confocal z-sections spaced by 0.62  $\mu\text{m}$  were collected every 3 minutes for 180 min, and projected to an  $xy$  image using a maximum intensity projection. Green, Myo3-S469V-3mYFP and Sid4-3mYFP; red, Rlc1-3mCherry. Bar, 5  $\mu\text{m}$ .



**Movie 6. Collapse of the Rlc1 ring in the *myo2-E1 myo3-S469V* background.** Related to the middle and bottom panels of Figure 5C. Strain: MTY780 (*myo2-E1 myo3-S469V-3mYFP rlc1-3mCherry sid4-3mYFP*). Time-lapse imaging of Myo3-S469V and Rlc1 rings using a confocal microscope (LSM 700; Carl Zeiss, Inc.) equipped with an alpha Plan-Apochromat 100 $\times$ /1.46 NA objective lens (Carl Zeiss, Inc.). Left and right columns correspond to the middle and bottom panels shown in Figure 5C, respectively. Stacks of 13 confocal *z*-sections spaced by 0.62  $\mu$ m were collected every 3 minutes for 180 min, and projected to an *xy* image using a maximum intensity projection. Green, Myo3-S469V-3mYFP and Sid4-3mYFP; red, Rlc1-3mCherry. Bar, 5  $\mu$ m.



**Movie 7. Behavior of Rlc1 rings in *myo3Δ cdc8-110* cells.** Related to Figure 6B. Strain: MTY983 (*cdc8-110 myo3Δ rlc1-3mYFP sid4-3mYFP*). Time-lapse imaging of the Rlc1 ring and SPBs using an inverted fluorescence microscope (BX71; Olympus) equipped with a UPlanSApo 100×/1.40 NA objective lens (Olympus), a spinning-disk confocal scanner (CSU22; Yokogawa), piezo objective positioner (E-665; Physik Instrumente), and electron multiplying CCD camera (iXon 3 885; Andor) with excitation by a 488-nm laser using a GFP filter and MetaMorph software (version 7.7.5.0; Molecular Devices). An asterisk indicates the cell shown in the bottom panel of Figure 6B. Stacks of 13 confocal *z*-sections spaced by 0.60  $\mu\text{m}$  were collected every 2 minutes for 240 min, and projected to an *xy* image using a maximum intensity projection. Bar, 5  $\mu\text{m}$ .



**Movie 8. Motile Myo3 clusters on the contractile ring.** Related to Figure 7D. Strains: MTY528 (*myo3-3mYFP sid4-3mYFP*) and MTY717 (*myo3-R694C-3mYFP sid4-3mYFP*).

Time-lapse imaging of the Myo3 ring and SPBs using an inverted fluorescence microscope (BX71; Olympus) equipped with a UPlanSApo 100×/1.40 NA objective lens (Olympus), spinning-disk confocal scanner (CSU22; Yokogawa), piezo objective positioner (E-665; Physik Instrumente), and electron multiplying CCD camera (iXon 3 885; Andor) with excitation by a 488-nm laser using a GFP filter and MetaMorph software (version 7.7.5.0; Molecular Devices). Asterisks indicate the cells shown in Figure 7D (the bottom panel for wt). Stacks of 9 confocal *z*-sections spaced by 0.31  $\mu\text{m}$  (corresponding to the lower half of the contractile ring) were collected every 15 s for 8 min. The stacked images were deconvolved using Huygens Essential software (version 4.5; Scientific Volume Imaging) based on the classic maximum likelihood estimation method, and projected to an *xy* image using a maximum intensity projection. Bar, 5  $\mu\text{m}$ .